

Search for Anomalous Production of Acoplanar Di-lepton Events in e^+e^- collisions at $\sqrt{s} = 183$ and 189 GeV

The OPAL Collaboration

Abstract

A selection of di-lepton events with significant missing transverse momentum has been performed using a total data sample of 237.4 pb^{-1} at e^+e^- centre-of-mass energies of 183 GeV and 189 GeV. The observed numbers of events — 78 at 183 GeV and 301 at 189 GeV — are consistent with the numbers expected from Standard Model processes, which arise predominantly from W^+W^- production with each W decaying leptonically. This topology is also an experimental signature for the pair production of new particles that decay to a charged lepton accompanied by one or more invisible particles. Discrimination techniques are described that optimise the sensitivity to particular new physics channels. No evidence for new phenomena is apparent and model independent limits are presented on the production cross-section times branching ratio squared for sleptons and for leptonically decaying charginos and charged Higgs. Assuming a 100% branching ratio for the decay $\tilde{\ell}_R^\pm \rightarrow \ell^\pm \tilde{\chi}_1^0$, where $\tilde{\chi}_1^0$ is the lightest neutralino, we exclude at 95% CL: right-handed smuons with masses below 82.3 GeV for $m_{\tilde{\mu}^-} - m_{\tilde{\chi}_1^0} > 3$ GeV and right-handed staus with masses below 81.0 GeV for $m_{\tilde{\tau}^-} - m_{\tilde{\chi}_1^0} > 8$ GeV. Right-handed selectrons are excluded at 95% CL for masses below 87.1 GeV for $m_{\tilde{e}^-} - m_{\tilde{\chi}_1^0} > 5$ GeV, within the framework of the Minimal Supersymmetric Standard Model assuming $\mu < -100$ GeV and $\tan \beta = 1.5$. Charged Higgs bosons, H^\pm , are excluded at 95% CL for masses below 82.8 GeV, assuming a 100% branching ratio for the decay $H^\pm \rightarrow \tau^\pm \nu_\tau$.

(To be submitted to Eur. Phys. J. C.)

The OPAL Collaboration

G. Abbiendi², K. Ackerstaff⁸, G. Alexander²³, J. Allison¹⁶, K.J. Anderson⁹, S. Anderson¹²,
S. Arcelli¹⁷, S. Asai²⁴, S.F. Ashby¹, D. Axen²⁹, G. Azuelos^{18,a}, A.H. Ball⁸, E. Barberio⁸,
R.J. Barlow¹⁶, J.R. Batley⁵, S. Baumann³, J. Bechtluft¹⁴, T. Behnke²⁷, K.W. Bell²⁰, G. Bella²³,
A. Bellerive⁹, S. Bentvelsen⁸, S. Bethke¹⁴, S. Betts¹⁵, O. Biebel¹⁴, A. Biguzzi⁵, I.J. Bloodworth¹,
P. Bock¹¹, J. Böhme¹⁴, O. Boeriu¹⁰, D. Bonacorsi², M. Boutemeur³³, S. Braibant⁸,
P. Bright-Thomas¹, L. Brigliadori², R.M. Brown²⁰, H.J. Burckhart⁸, P. Capiluppi²,
R.K. Carnegie⁶, A.A. Carter¹³, J.R. Carter⁵, C.Y. Chang¹⁷, D.G. Charlton^{1,b}, D. Chrisman⁴,
C. Ciocca², P.E.L. Clarke¹⁵, E. Clay¹⁵, I. Cohen²³, J.E. Conboy¹⁵, O.C. Cooke⁸, J. Couchman¹⁵,
C. Couyoumtzelis¹³, R.L. Coxe⁹, M. Cuffiani², S. Dado²², G.M. Dallavalle², S. Dallison¹⁶,
R. Davis³⁰, S. De Jong¹², A. de Roeck⁸, P. Dervan¹⁵, K. Desch²⁷, B. Dienes^{32,h}, M.S. Dixit⁷,
M. Donkers⁶, J. Dubbert³³, E. Duchovni²⁶, G. Duckeck³³, I.P. Duerdoth¹⁶, P.G. Estabrooks⁶,
E. Etzion²³, F. Fabbri², A. Fanfani², M. Fanti², A.A. Faust³⁰, L. Feld¹⁰, P. Ferrari¹²,
F. Fiedler²⁷, M. Fierro², I. Fleck¹⁰, A. Frey⁸, A. Fürstjes⁸, D.I. Futyan¹⁶, P. Gagnon⁷,
J.W. Gary⁴, G. Gaycken²⁷, C. Geich-Gimbel³, G. Giacomelli², P. Giacomelli², W.R. Gibson¹³,
D.M. Gingrich^{30,a}, D. Glenzinski⁹, J. Goldberg²², W. Gorn⁴, C. Grandi², K. Graham²⁸,
E. Gross²⁶, J. Grunhaus²³, M. Gruwé²⁷, C. Hajdu³¹, G.G. Hanson¹², M. Hansroul⁸, M. Hapke¹³,
K. Harder²⁷, A. Harel²², C.K. Hargrove⁷, M. Harin-Dirac⁴, M. Hauschild⁸, C.M. Hawkes¹,
R. Hawkings²⁷, R.J. Hemingway⁶, G. Herten¹⁰, R.D. Heuer²⁷, M.D. Hildreth⁸, J.C. Hill⁵,
P.R. Hobson²⁵, A. Hocker⁹, K. Hoffman⁸, R.J. Homer¹, A.K. Honma^{28,a}, D. Horváth^{31,c},
K.R. Hossain³⁰, R. Howard²⁹, P. Hüntemeyer²⁷, P. Igo-Kemenes¹¹, D.C. Imrie²⁵, K. Ishii²⁴,
F.R. Jacob²⁰, A. Jawahery¹⁷, H. Jeremie¹⁸, M. Jimack¹, C.R. Jones⁵, P. Jovanovic¹, T.R. Junk⁶,
N. Kanaya²⁴, J. Kanzaki²⁴, D. Karlen⁶, V. Kartvelishvili¹⁶, K. Kawagoe²⁴, T. Kawamoto²⁴,
P.I. Kayal³⁰, R.K. Keeler²⁸, R.G. Kellogg¹⁷, B.W. Kennedy²⁰, D.H. Kim¹⁹, A. Klier²⁶,
T. Kobayashi²⁴, M. Kobel³, T.P. Kokott³, M. Kolrep¹⁰, S. Komamiya²⁴, R.V. Kowalewski²⁸,
T. Kress⁴, P. Krieger⁶, J. von Krogh¹¹, T. Kuhl³, P. Kyberd¹³, G.D. Lafferty¹⁶, H. Landsman²²,
D. Lanske¹⁴, J. Lauber¹⁵, I. Lawson²⁸, J.G. Layter⁴, D. Lellouch²⁶, J. Letts¹², L. Levinson²⁶,
R. Liebisch¹¹, J. Lillich¹⁰, B. List⁸, C. Littlewood⁵, A.W. Lloyd¹, S.L. Lloyd¹³, F.K. Loebinger¹⁶,
G.D. Long²⁸, M.J. Losty⁷, J. Lu²⁹, J. Ludwig¹⁰, D. Liu¹², A. Macchiolo¹⁸, A. Macpherson³⁰,
W. Mader³, M. Mannelli⁸, S. Marcellini², T.E. Marchant¹⁶, A.J. Martin¹³, J.P. Martin¹⁸,
G. Martinez¹⁷, T. Mashimo²⁴, P. Mättig²⁶, W.J. McDonald³⁰, J. McKenna²⁹, E.A. Mckigney¹⁵,
T.J. McMahon¹, R.A. McPherson²⁸, F. Meijers⁸, P. Mendez-Lorenzo³³, F.S. Merritt⁹, H. Mes⁷,
I. Meyer⁵, A. Michelini², S. Mihara²⁴, G. Mikenberg²⁶, D.J. Miller¹⁵, W. Mohr¹⁰, A. Montanari²,
T. Mori²⁴, K. Nagai⁸, I. Nakamura²⁴, H.A. Neal^{12,f}, R. Nisius⁸, S.W. O'Neale¹, F.G. Oakham⁷,
F. Odorici², H.O. Ogren¹², A. Okpara¹¹, M.J. Oreglia⁹, S. Orito²⁴, G. Pásztor³¹, J.R. Pater¹⁶,
G.N. Patrick²⁰, J. Patt¹⁰, R. Perez-Ochoa⁸, S. Petzold²⁷, P. Pfeifenschneider¹⁴, J.E. Pilcher⁹,
J. Pinfold³⁰, D.E. Plane⁸, P. Poffenberger²⁸, B. Poli², J. Polok⁸, M. Przybycień^{8,d}, A. Quadt⁸,
C. Rembser⁸, H. Rick⁸, S. Robertson²⁸, S.A. Robins²², N. Rodning³⁰, J.M. Roney²⁸, S. Rosati³,
K. Roscoe¹⁶, A.M. Rossi², Y. Rozen²², K. Runge¹⁰, O. Runolfsson⁸, D.R. Rust¹², K. Sachs¹⁰,
T. Saeki²⁴, O. Sahr³³, W.M. Sang²⁵, E.K.G. Sarkisyan²³, C. Sbarra²⁹, A.D. Schaile³³,
O. Schaile³³, P. Scharff-Hansen⁸, J. Schieck¹¹, S. Schmitt¹¹, A. Schöning⁸, M. Schröder⁸,
M. Schumacher³, C. Schwick⁸, W.G. Scott²⁰, R. Seuster¹⁴, T.G. Shears⁸, B.C. Shen⁴,
C.H. Shepherd-Themistocleous⁵, P. Sherwood¹⁵, G.P. Siroli², A. Skuja¹⁷, A.M. Smith⁸,
G.A. Snow¹⁷, R. Sobie²⁸, S. Söldner-Rembold^{10,e}, S. Spagnolo²⁰, M. Sproston²⁰, A. Stahl³,
K. Stephens¹⁶, K. Stoll¹⁰, D. Strom¹⁹, R. Ströhmer³³, B. Surrow⁸, S.D. Talbot¹, P. Taras¹⁸,

S. Tarem²², R. Teuscher⁹, M. Thiergen¹⁰, J. Thomas¹⁵, M.A. Thomson⁸, E. Torrence⁸, S. Towers⁶, T. Trefzger³³, I. Trigger¹⁸, Z. Trócsányi^{32,g}, E. Tsur²³, M.F. Turner-Watson¹, I. Ueda²⁴, R. Van Kooten¹², P. Vannerem¹⁰, M. Verzocchi⁸, H. Voss³, F. Wäckerle¹⁰, A. Wagner²⁷, D. Waller⁶, C.P. Ward⁵, D.R. Ward⁵, P.M. Watkins¹, A.T. Watson¹, N.K. Watson¹, P.S. Wells⁸, N. Wermes³, D. Wetterling¹¹, J.S. White⁶, G.W. Wilson¹⁶, J.A. Wilson¹, T.R. Wyatt¹⁶, S. Yamashita²⁴, V. Zacek¹⁸, D. Zer-Zion⁸

¹School of Physics and Astronomy, University of Birmingham, Birmingham B15 2TT, UK

²Dipartimento di Fisica dell' Università di Bologna and INFN, I-40126 Bologna, Italy

³Physikalisches Institut, Universität Bonn, D-53115 Bonn, Germany

⁴Department of Physics, University of California, Riverside CA 92521, USA

⁵Cavendish Laboratory, Cambridge CB3 0HE, UK

⁶Ottawa-Carleton Institute for Physics, Department of Physics, Carleton University, Ottawa, Ontario K1S 5B6, Canada

⁷Centre for Research in Particle Physics, Carleton University, Ottawa, Ontario K1S 5B6, Canada

⁸CERN, European Organisation for Particle Physics, CH-1211 Geneva 23, Switzerland

⁹Enrico Fermi Institute and Department of Physics, University of Chicago, Chicago IL 60637, USA

¹⁰Fakultät für Physik, Albert Ludwigs Universität, D-79104 Freiburg, Germany

¹¹Physikalisches Institut, Universität Heidelberg, D-69120 Heidelberg, Germany

¹²Indiana University, Department of Physics, Swain Hall West 117, Bloomington IN 47405, USA

¹³Queen Mary and Westfield College, University of London, London E1 4NS, UK

¹⁴Technische Hochschule Aachen, III Physikalisches Institut, Sommerfeldstrasse 26-28, D-52056 Aachen, Germany

¹⁵University College London, London WC1E 6BT, UK

¹⁶Department of Physics, Schuster Laboratory, The University, Manchester M13 9PL, UK

¹⁷Department of Physics, University of Maryland, College Park, MD 20742, USA

¹⁸Laboratoire de Physique Nucléaire, Université de Montréal, Montréal, Quebec H3C 3J7, Canada

¹⁹University of Oregon, Department of Physics, Eugene OR 97403, USA

²⁰CLRC Rutherford Appleton Laboratory, Chilton, Didcot, Oxfordshire OX11 0QX, UK

²²Department of Physics, Technion-Israel Institute of Technology, Haifa 32000, Israel

²³Department of Physics and Astronomy, Tel Aviv University, Tel Aviv 69978, Israel

²⁴International Centre for Elementary Particle Physics and Department of Physics, University of Tokyo, Tokyo 113-0033, and Kobe University, Kobe 657-8501, Japan

²⁵Institute of Physical and Environmental Sciences, Brunel University, Uxbridge, Middlesex UB8 3PH, UK

²⁶Particle Physics Department, Weizmann Institute of Science, Rehovot 76100, Israel

²⁷Universität Hamburg/DESY, II Institut für Experimental Physik, Notkestrasse 85, D-22607 Hamburg, Germany

²⁸University of Victoria, Department of Physics, P O Box 3055, Victoria BC V8W 3P6, Canada

²⁹University of British Columbia, Department of Physics, Vancouver BC V6T 1Z1, Canada

³⁰University of Alberta, Department of Physics, Edmonton AB T6G 2J1, Canada

³¹Research Institute for Particle and Nuclear Physics, H-1525 Budapest, P O Box 49, Hungary

³²Institute of Nuclear Research, H-4001 Debrecen, P O Box 51, Hungary

³³Ludwigs-Maximilians-Universität München, Sektion Physik, Am Coulombwall 1, D-85748 Garching, Germany

^a and at TRIUMF, Vancouver, Canada V6T 2A3

^b and Royal Society University Research Fellow

^c and Institute of Nuclear Research, Debrecen, Hungary

^d and University of Mining and Metallurgy, Cracow

^e and Heisenberg Fellow

^f now at Yale University, Dept of Physics, New Haven, USA

^g and Department of Experimental Physics, Lajos Kossuth University, Debrecen, Hungary.

1 Introduction

We report on a set of selected events containing two oppositely charged leptons and significant missing transverse momentum. Data are analysed from e^+e^- collisions at LEP at centre-of-mass energies of 182.7 and 188.7 GeV with integrated luminosities corresponding to 56.4 pb^{-1} and 181.0 pb^{-1} , respectively. The number of observed events and their studied properties are found to be consistent with the expectations for Standard Model processes, which are dominated by the $\ell^+\nu\ell^-\bar{\nu}$ final state ($\ell = e, \mu, \tau$) arising from W^+W^- production in which both W bosons decay leptonically: $W^- \rightarrow \ell^-\bar{\nu}_\ell$.

This topology is also an experimental signature for the pair production of new particles that decay to produce a charged lepton accompanied by one or more invisible particles, such as neutrinos or the hypothesised lightest stable supersymmetric [1] particle (LSP), which may be the lightest neutralino, $\tilde{\chi}_1^0$, or the gravitino, \tilde{G} . Experimentally, invisible particles may also be weakly interacting neutral particles with long lifetimes, which decay outside the detector volume. We present the results of searches for the following new particle decays:

charged scalar leptons (sleptons): $\tilde{\ell}^\pm \rightarrow \ell^\pm \tilde{\chi}_1^0$ (or $\tilde{\ell}^\pm \rightarrow \ell^\pm \tilde{G}$), where $\tilde{\ell}^\pm$ may be a selectron (\tilde{e}), smuon ($\tilde{\mu}$) or stau ($\tilde{\tau}$) and ℓ^\pm is the corresponding charged lepton.

charged Higgs: $H^\pm \rightarrow \tau^\pm \nu_\tau$.

charginos: $\tilde{\chi}_1^\pm \rightarrow \ell^\pm \tilde{\nu}$ (“2-body” decays) or $\tilde{\chi}_1^\pm \rightarrow \ell^\pm \nu \tilde{\chi}_1^0$ (“3-body” decays).

The search for charged scalar leptons provides constraints on the selectron mass and indirectly the electron-sneutrino mass (in models where these are related). These searches are therefore also relevant to interpreting the results of searches for chargino and neutralino production since the production cross-section and branching ratios depend on the slepton masses.

In most respects the analysis is similar to our published searches at centre-of-mass energies of 161, 172 and 183 GeV [2, 3]. The analysis is performed in two stages. The first stage consists of a general selection for all possible events containing a lepton pair plus missing transverse momentum (Section 3). In this context the Standard Model $\ell^+\nu\ell^-\bar{\nu}$ events are considered as signal in addition to the possible new physics sources. All Standard Model processes that do not lead to $\ell^+\nu\ell^-\bar{\nu}$ final states — e.g. $e^+e^-\ell^+\ell^-$ and $\ell^+\ell^-(\gamma)$ — are considered as background and are reduced to a rather low level by the event selection. In the second stage the detailed properties of the events (e.g. the type of leptons observed and their momenta), which vary greatly depending on the type of new particles considered and on free parameters within the models, are used to separate as far as possible the events consistent with potential new physics sources from W^+W^- and other Standard Model processes (Section 4).

The other LEP collaborations have published searches for sleptons in this channel using data at $\sqrt{s} \leq 183 \text{ GeV}$ [4].

In this paper we describe fully only those aspects in which the second stage of the analysis differs significantly from [3]. These are:

- The use of the acolinearity of the event as an additional likelihood variable, and use of the fact that the momentum distributions employed in the likelihood calculation vary with acolinearity.

- The use of an extended maximum likelihood technique to calculate the upper limits on the cross-section times branching ratio squared.

2 OPAL Detector and Monte Carlo Simulation

A detailed description of the OPAL detector can be found elsewhere [5].

The central detector consists of a system of chambers providing charged particle tracking over 96% of the full solid angle inside a 0.435 T uniform magnetic field parallel to the beam axis. It consists of a two-layer silicon micro-strip vertex detector, a high precision drift chamber, a large volume jet chamber and a set of z -chambers that measure the track coordinates along the beam direction.

A lead-glass electromagnetic calorimeter is located outside the magnet coil. It provides, in combination with the forward detectors, which are lead-scintillator sandwich calorimeters and, at smaller angles, silicon tungsten calorimeters, geometrical acceptance with excellent hermeticity down to approximately 25 mrad.

The magnet return yoke is instrumented for hadron calorimetry and consists of barrel and endcap sections along with pole tip detectors that together cover the region $|\cos\theta| < 0.99$. Outside the hadron calorimeter, four layers of muon chambers cover the polar angle range of $|\cos\theta| < 0.98$. Arrays of thin scintillating tiles have been installed in the endcap region to improve trigger performance, time resolution and hermeticity for experiments at LEP 2 [6]. Of particular relevance to this analysis are the four layers of scintillating tiles (the MIP plug) installed at each end of the OPAL detector covering the angular range $43 < \theta < 220$ mrad.

The following Standard Model processes are simulated. 4-fermion production is simulated using the grc4f [7] generator at $\sqrt{s}=183$ GeV, and using the KORALW [8] generator at $\sqrt{s}=189$ GeV. KORALW uses the grc4f matrix elements to calculate the four-fermion cross-sections including interference effects and includes a detailed description of hard radiation from initial, intermediate and final state charged particles. Two-photon processes are generated using the program of Vermaseren [10] and grc4f for $e^+e^-\ell^+\ell^-$, and using PHOJET [11], HERWIG [12] and grc4f for $e^+e^-q\bar{q}$. Because of the large total cross-section for $e^+e^-e^+e^-$, $e^+e^-\mu^+\mu^-$ and $e^+e^-q\bar{q}$, soft cuts are applied at the generator level to preselect events that might possibly lead to background in the selection of $\ell^+\nu\ell^-\bar{\nu}$ final states. No generator level cuts are applied to the $e^+e^-\tau^+\tau^-$ generation. The production of lepton pairs is generated using BHWIDE [13] and TEEGG [14] for $e^+e^-(\gamma)$, and using KORALZ [15] for $\mu^+\mu^-(\gamma)$ and $\tau^+\tau^-(\gamma)$. The production of quark pairs, $q\bar{q}(g)$, is generated using PYTHIA [16] and the final state $\nu\bar{\nu}\gamma\gamma$ is generated using NUNUGPV98 [17] and KORALZ.

Slepton pair production is generated using SUSYGEN [18]. Chargino pair production is generated using DFGT [19] for three-body decays, and SUSYGEN for two-body decays. Charged Higgs boson pair production is generated using HZHA [20] and PYTHIA.

All Standard Model and new physics Monte Carlo samples are processed with a full simulation of the OPAL detector [21] and subjected to the same reconstruction and analysis programs as used for the OPAL data.

3 General Selection of Di-lepton Events with Significant Missing Momentum

The general selection of acoplanar lepton pair events, which selects events containing low multiplicity jets with significant missing transverse momentum, p_t^{miss} , is described in detail in [2]. In [3] we made use of the improved hermeticity for non-showering particles in the forward direction provided by the MIP plug. Subsequent modifications have been made for the analysis of the data taken at 189 GeV, the most important of which was prompted by Monte Carlo studies which showed that, in the majority of Standard Model background events (non $\ell^+\nu\ell^-\bar{\nu}$) accepted by the general selection, p_t^{miss} was overestimated due to the mis-measurement of tracks and clusters. In the current analysis the uncertainty on p_t^{miss} is calculated from the measurement uncertainty on the observed tracks and clusters, and the requirement in [2] that p_t^{miss} exceed certain fixed cuts is replaced by the requirement that it exceed the cut values by at least one standard deviation of the calculated measurement uncertainty. These changes – both the MIP-plug cut and the p_t^{miss} significance, have markedly reduced the residual backgrounds and have allowed the selection efficiency to be substantially increased by removing many of the cuts of selection II which are now redundant. In brief, the essence of event selection II is now :

- $p_t^{\text{miss}}/E_{\text{beam}}$ should significantly exceed 0.05.
- The scaled missing transverse momentum with respect to the transverse thrust axis, $a_t^{\text{miss}}/E_{\text{beam}}$ should exceed 0.022 for events with low acoplanarity.
- Events with values of $p_t^{\text{miss}}/E_{\text{beam}}$ which could potentially be balanced by beam energy muons in the MIP-plug acceptance are rejected if evidence for such forward-going particles is seen in these scintillators.

The numbers of events passing the general selection at each centre-of-mass energy in the data are compared to the Standard Model Monte Carlo predictions in Table 1. The total number of events predicted by the Standard Model is given, together with a breakdown into the contributions from individual processes. The number of observed candidates is consistent with the expectation from Standard Model sources, which is dominated by the $\ell^+\nu\ell^-\bar{\nu}$ final state arising mostly from W^+W^- production in which both W 's decay leptonically: $W^- \rightarrow \ell^-\bar{\nu}_\ell$.

\sqrt{s} (GeV)	data	SM	$\ell^+\nu\ell^-\bar{\nu}$	$e^+e^-\ell^+\ell^-$	$\ell\ell q\bar{q}$	$\ell^+\ell^-(\gamma)$	$\nu\bar{\nu}\gamma\gamma$
183	78	81.4±0.8	77.5±0.7	3.4±0.5	0.07±0.03	0.31±0.04	0.06±0.03
189	301	303.3±1.9	292.5±1.6	4.4±0.8	1.3±0.1	4.6±0.4	0.46±0.04

Table 1: Comparison between data and Monte Carlo of the number of events passing the general selection at each centre-of-mass energy. The total number of events predicted by the Standard Model is given, together with a breakdown into the contributions from individual processes. The Monte Carlo statistical errors are shown.

The second stage of the analysis, in which we distinguish between Standard Model and new physics sources of lepton pair events with missing momentum, is described in Section 4. Discrimination is provided by information on the lepton identification, the acolinearity of the event, and the momentum and $-q \cos \theta$ of the observed lepton candidates, where q and θ are

Lepton identification	$\sqrt{s}=189$ GeV		$\sqrt{s}=183$ GeV	
	data	SM	data	SM
e^+e^-	49	45.2±0.7	14	12.1±0.3
$\mu^+\mu^-$	49	47.0±0.7	13	13.7±0.3
$h^\pm h^\mp$	16	11.0±0.5	1	2.5±0.2
$e^\pm \mu^\mp$	79	83.4±0.9	20	25.6±0.4
$e^\pm h^\mp$	26	36.6±0.6	8	9.8±0.3
$\mu^\pm h^\mp$	40	35.4±0.6	8	9.2±0.2
e^\pm , unidentified	20	19.6±0.7	5	3.8±0.2
μ^\pm , unidentified	14	17.8±0.5	7	3.7±0.2
h^\pm , unidentified	8	7.3±0.3	2	0.9±0.1

Table 2: *The lepton identification information in the events passing the general selection compared with the Standard Model Monte Carlo at each centre-of-mass energy. “h” means that the lepton is identified neither as an electron nor muon and so is probably the product of a hadronic tau decay. Leptonic decays of taus are usually classified as electron or muon. “Unidentified” means that only one isolated lepton has been positively identified in the event.*

the charge and polar production angle of the lepton. We check here on the degree to which these quantities are described by the Standard Model Monte Carlo. The lepton identification information in the event sample produced by the general selection at each centre-of-mass energy is compared with the Standard Model Monte Carlo in Table 2. For the event sample at $\sqrt{s}=189$ GeV, Figure 1 shows the distributions of (a) the momentum scaled by the beam energy of each charged lepton candidate, (b) the value of $-q \cos \theta$ of each charged lepton candidate, and (c) the acolinearity of the event. The data are compared with the Standard Model Monte Carlo predictions, which are dominated by the final state $\ell^+\nu \ell^-\bar{\nu}$.

The cuts used to veto two-photon background introduce an inefficiency in the event selection due to random detector occupancy (principally in the SW, FD and MIP plug detectors) that is not modelled in the Monte Carlo. This inefficiency has been measured using randomly triggered events collected during normal data taking. For events with very low missing transverse momentum the inefficiency has a value of 8.3% at $\sqrt{s} = 189$ GeV and 8.2% at $\sqrt{s} = 183$ GeV for events, and decreases to a negligible value for events with $p_t^{\text{miss}}/E_{\text{beam}} > 0.25$. When quoting expected numbers of Standard Model events and selection efficiencies for potential new physics sources, the variation of veto inefficiency with p_t^{miss} is taken into account.

4 Likelihood Method to Distinguish Signal and Background

Starting from the general selection of acoplanar di-lepton events, we search for the production of new particles by using a likelihood technique which combines the information from a number of discriminating variables in order to distinguish between new physics signals and Standard Model sources of such events, the most important of which are $\ell^+\nu \ell^-\bar{\nu}$ and $e^+e^- \ell^+\ell^-$.

Discrimination between new particle pair production and the Standard Model background is performed by considering the likelihood that an event is consistent with being either signal

or background. Given an event, for which the values of a set of variables x_i are known, the likelihood, L_S , of the event being consistent with the signal hypothesis is calculated as the product of the probabilities, $P_S(x_i)$, that the signal hypothesis would produce an event with variable i having value x_i , $L_S = \prod_i P_S(x_i)$. Similarly, the likelihood of an event being consistent with the background hypothesis is $L_B = \prod_i P_B(x_i)$. The discriminating quantity used is the relative likelihood, L_R , defined by:

$$L_R = \frac{L_S}{L_S + L_B}.$$

An event with high L_R is signal-like and an event with low L_R is background-like.

The following quantities are used as likelihood variables (x_i) in the analysis:

- (i) Scaled momentum, p/E_{beam} , of each lepton,
- (ii) Acolinearity of the event, defined as the supplement of the 3-D angle between the two leptons.
- (iii) $-q \cos \theta$ for each lepton (smuons, staus and charged Higgs only),
- (iv) Lepton type variable (defined in Section 4.4).

Sections 4.1 to 4.4 describe the properties of each of these variables for signal and background.

4.1 The Momentum Likelihood Variable

The dominant Standard Model process leading to the acoplanar di-lepton signature arises from leptonically decaying W pairs, and the momentum distribution is highly populated between about 0.25 and 0.7 (Figure 1(a)). The kinematics for the signal vary considerably with the mass difference, Δm , between the parent particle (e.g. selectron) and the invisible daughter particle (e.g. $\tilde{\chi}_1^0$), since this determines how much energy is available to the lepton. The kinematics also vary to a lesser extent with the mass m of the parent particle, due to Lorentz boost effects.

A significant change to the analysis with respect to earlier publications is the inclusion of the fact that for a given m and Δm , the lepton momentum distribution varies according to the acolinearity of the event. Since the parent particles (e.g. sleptons) are produced back to back, then if an event has high acolinearity, one of the leptons will typically be travelling in a direction at an angle greater than $\pi/2$ to that of the parent particle (in the lab. frame). In this case, the lepton momentum in the lab. frame is reduced relative to its value in the rest frame of the parent particle and the lepton is therefore soft. An event with low acolinearity will in general have both leptons travelling in similar directions to the parent particles and the Lorentz boost results in both leptons having high momenta, provided that the parent particle mass is not close to the kinematic limit. Since the Lorentz boost is stronger for low parent particle mass, these effects are greater when m is small.

Figure 2 shows momentum distributions in the (x_{max}, x_{min}) plane, where x_{max} and x_{min} are the scaled momenta of the higher and lower momentum leptons, respectively, for a smuon

signal with $m=45$ GeV, $\Delta m=45$ GeV, for 3 different ranges of acolinearity. The corresponding plots for background are also shown.

Signal and Standard Model Monte Carlos are used to construct reference histograms for momentum in a grid of points in the $(m, \Delta m)$ plane, with m ranging from 45 to 94 GeV, and Δm ranging from 2 GeV to m . Each of the signal momentum distributions and the background distribution is subdivided into the following 3 ranges of acolinearity (in radians): $0 \leq \theta_{acol} < 0.8$, $0.8 \leq \theta_{acol} < 1.6$ and $1.6 \leq \theta_{acol} < \pi$. Each of these distributions is then further subdivided according to whether the observed lepton is the higher or lower momentum lepton.

For the searches in which the final state particles can be the decay products of taus (staus, charginos and charged Higgs), each momentum probability distribution must be further subdivided, as the momentum spectrum depends on the lepton identification. One momentum probability distribution is constructed for the case in which the observed lepton is identified as e or μ , and another for the case in which the observed lepton is identified as a hadronically decaying tau, or is unidentified.

Probabilities $P_S(x_i)$ and $P_B(x_i)$ for the likelihood calculation are found by reading from the appropriate reference histograms.

4.2 The Acolinearity Likelihood Variable

For signal, the distribution of the acolinearity angle varies with m and Δm . For low parent particle mass, the Lorentz boost results in a tendency for the leptons to be in the directions of the parent particles, resulting in the acolinearity being peaked towards low values, whereas for high mass, the parent particles are produced close to being at rest, and the leptons have no preferred direction. For background, the acolinearity distribution is peaked towards low values due to the spin structure of the weak couplings.

Figure 3 shows some example acolinearity distributions for signal, which can be compared to the distributions for background and data shown in Figure 1.

The use of the acolinearity as a likelihood variable is complementary to its use in defining the momentum probability, in that the masses for which it offers the greatest discrimination as a likelihood variable are the masses where the gain in distinguishing power described in Section 4.1 is small, and vice versa.

4.3 The $-q \cos \theta$ Likelihood Variable

As described in [3], the distribution of the quantity $-q \cos \theta$, where q and θ are the charge and production angle of an observed lepton, is forward peaked for W^+W^- production due to the dominance of the neutrino exchange amplitude and the V-A nature of W decay, whereas for smuon, stau and charged Higgs production the distribution is symmetric and peaked towards $|\cos \theta| = 0$, due to the scalar nature of these particles.

This variable is not used in the likelihood calculation for selectrons or charginos because these particles can be produced via t -channel neutralino exchange and sneutrino exchange, respectively, in addition to s -channel production. This results in the expected $-q \cos \theta$ distribution of selectrons and charginos being model-dependent and potentially similar to that of the W^+W^- background.

4.4 The Lepton Type Likelihood Variable

A value is assigned to the lepton type variable according to which types of lepton are identified in the event. There are nine possible values, corresponding to the nine event types listed in table 2.

For the selectron (smuon) analysis a cut is applied at the same time as the general selection, requiring at least one electron (muon) and no muons (electrons), reducing the background by about 2/3 (depending on slepton type and \sqrt{s}) with negligible loss of efficiency. With this cut applied, there are only three possible values of the lepton type variable.

4.5 L_R and L_B Distributions

For each search channel, reference histograms are constructed for each of the likelihood variables at each point in m and Δm for which signal Monte Carlo has been generated. A smoothing algorithm [22] is applied to the histograms to reduce the effects of statistical fluctuations. The reference histograms are then used to construct L_R distributions.

L_R distributions for signal Monte Carlo, Standard Model Monte Carlo and data are shown in Figure 4 for the specific example of the analysis for smuons with a mass of 80 GeV and a smuon-neutralino mass difference of 60 GeV. There is considerable variation in the shapes of these distributions with m and Δm .

A check of consistency between data and the Standard Model can be performed without reference to a particular signal by comparing the L_B distributions for data and Standard Model. Figure 5(a) shows the L_B distributions for the Standard Model (histogram) and data (points) for events passing the general selection. All the likelihood variables are used. Figures 5(b) and (c) show the same information after making the initial lepton identification requirements given in Section 4.4 for the selectron and smuon searches respectively. In Figure 5(b), only the variables used in the selectron analysis are used. In each of the plots, the secondary peak at high L_B corresponds to events which have only one identified lepton and therefore fewer variables entering the likelihood ¹. In all three plots, the data is in good agreement with the Standard Model.

5 Calculation of Cross-Section Limits

5.1 Introduction

In [3], the limit on the cross-section was calculated by finding an optimised cut on the value of L_R as a function of m and Δm for each centre of mass energy, and applying this cut to signal Monte Carlo, Standard Model Monte Carlo and data. The resulting efficiencies, expected backgrounds and numbers of candidates were used to calculate cross-section limits using the likelihood ratio method [23] to combine the information.

In this paper, we describe the use of an extended maximum likelihood calculation to determine the cross-section limits. In this method, no cut is applied on L_R . Information contained

¹This effect cancels when the likelihood ratio L_R is calculated because the events will have high L_S for the same reason.

in the L_R values of each individual candidate event, and in the shapes of the L_R distributions for signal and background are used as input to the limit calculation, rather than the numbers of events passing a cut. In this way, considerably more of the available information is used.

The advantage of a cut free method can be seen by considering, for example, a case where there is an excess of candidates passing a cut on L_R . The information about whether the events all lie close to the cut, or whether they are clustered towards $L_R=1$ (suggesting the presence of a signal) is not used. The use of the additional information makes the analysis more sensitive for discovery, and at the same time is able to set more stringent limits in the absence of signal. The expected sensitivity (ie., the expected upper limit on the cross-section) is improved by as much as 20%, depending on m and Δm , using this technique.

5.2 Extended Maximum Likelihood Technique

The upper limit on the cross-section times branching ratio squared at 95% confidence level, σ_{95} , is calculated by forming a likelihood, $L(\sigma_s)$, of the set of L_R values for the data being consistent with the expected L_R distribution for Standard Model plus a signal produced with cross-section times branching ratio squared σ_s . σ_{95} is the value of σ_s below which 95% of the area under the likelihood function lies.

5.2.1 The Likelihood Function

Extended maximum likelihood combines standard maximum likelihood with the Poisson probability of observing N candidate events when ν are expected:

$$L = \frac{e^{-\nu} \nu^N}{N!} \prod_{i=1}^N P(L_{R_i}; B, S),$$

where $P(L_{R_i}; B, S)$ is the probability of event i having $L_R = L_{R_i}$, given L_R distributions B and S for background and signal.

Dropping the constant $N!$, this can be re-written:

$$\ln L = -\nu + \sum_{i=1}^N \ln[Q(L_{R_i}; B, S)]$$

where Q is identical to P but normalised to ν instead of 1 ($Q = \nu P$).

The expected number of candidates ν is given by:

$$\nu = \mu_B + \epsilon \mathcal{L} \omega \sigma_s,$$

where μ_B is the expected number of Standard Model events with non-zero L_R passing the general selection (similarly, N is the number of data candidates with $L_R \neq 0$), ϵ is the signal selection efficiency of the general selection, \mathcal{L} is the experimental luminosity and ω is a weight

factor which takes into account that the expected production cross-section varies with \sqrt{s} , but the limit on the observed cross-section is quoted at $\sqrt{s} = 189$ GeV.

$$\omega_i = \frac{\sigma_i}{\sigma_{189}},$$

where σ_{189} is the expected cross-section for $\sqrt{s} = 189$ GeV and σ_i is the expected cross-section for the i 'th value of \sqrt{s} . For scalar particles, for example sleptons, we assume that the expected cross-section varies as β^3/s . For spin $\frac{1}{2}$ particles, for example charginos, we assume that the expected cross-section varies as β/s .

The function Q is the probability of event i having $L_R = L_{R_i}$, given L_R distributions B and S for background and signal, normalised to ν . This is given by:

$$Q = \mu_B B(L_{R_i}) + \epsilon \mathcal{L} \omega \sigma_s S(L_{R_i}),$$

where the functions B and S , formed using background and signal Monte Carlo respectively, are normalised to 1.

Hence the likelihood function is given by:

$$\ln L(\sigma_s) = -(\mu_B + \epsilon \mathcal{L} \omega \sigma_s) + \sum_{i=1}^N \ln[\mu_B B(L_{R_i}) + \epsilon \mathcal{L} \omega \sigma_s S(L_{R_i})].$$

5.2.2 Limit Calculation

For data at a single centre-of-mass energy, the upper limit on the cross-section at 95% confidence level is the value of σ_{95} which satisfies:

$$0.95 = \frac{\int_0^{\sigma_{95}} L(\sigma_s) d\sigma_s}{\int_0^{\infty} L(\sigma_s) d\sigma_s}.$$

The generalisation to N_{ECM} values of \sqrt{s} is:

$$0.95 = \frac{\int_0^{\sigma_s^{189}} \prod_{i=1}^{N_{ECM}} L_i(\sigma_s^{189}) d\sigma_s^{189}}{\int_0^{\infty} \prod_{i=1}^{N_{ECM}} L_i(\sigma_s^{189}) d\sigma_s^{189}}.$$

where σ_s^{189} is the cross-section at $\sqrt{s} = 189$ GeV.

5.2.3 Verification of the Method

The technique used to calculate limits was tested using a toy Monte Carlo to simulate data sets for an ensemble of simulated experiments in which a signal is present with cross-section σ_s . The total number of candidates was drawn from a Poisson distribution with mean ν and for each candidate, a value of L_R was assigned, chosen randomly according to the sum of the expected L_R distributions for background and signal with cross-section σ_s .

σ_{95} was calculated for 500 simulated experiments. This was done using smuon signals at all m and Δm for which Monte Carlo has been generated, for 189 GeV separately and for 183 GeV and 189 GeV combined, and for a number of values of σ_s . In all cases, 95% of the 500 σ_{95} values were found to be greater than the true cross-section σ_s , to within the statistical error expected from the finite number of simulated experiments.

As a further test, the best estimate of the signal cross-section, σ_{best} , was calculated for each simulated experiment. This is the value of σ_s at which the likelihood function $L_i(\sigma_s)$ peaks. The σ_{best} distribution from the 500 simulated experiments was in all cases found to peak at the true cross-section.

5.3 Limit Calculation at an Arbitrary Point in m and Δm

Monte Carlo signal events are available only at certain particular values of m and Δm . The values of m range typically from $m = 45 \text{ GeV}$ ² up to $m \approx E_{\text{beam}}$ in 5 GeV steps. The values of Δm vary between 2 and $\Delta m = m$. In order to calculate σ_{95} at an intermediate point in m and Δm , it is necessary to be able to calculate L_R at that point for a given event, which requires the existence of reference histograms for the likelihood variables for any m and Δm .

An algorithm has been developed to construct the reference histograms at any intermediate value of m and Δm , given the histograms at the four nearest signal Monte Carlo grid points, assuming a linear variation in the shape of the histograms with m and Δm . This procedure has been tested by re-constructing histograms at gridpoints using the histograms at adjacent gridpoints.

For a given point m and Δm , the signal and background L_R distributions and the data L_R values are calculated using the interpolated reference histograms. Signal Monte Carlo at an intermediate point is simulated using signal Monte Carlo events at the nearest grid point. This is done by re-defining the value of each likelihood variable for an event, such that the fraction of the corresponding reference histogram at the intermediate point which lies below the re-defined value is the same as the fraction of the histogram at the grid point which lies below the original value.

The effects of statistical fluctuations in the L_R distributions are reduced using the same smoothing algorithm as applied to the reference histograms (section 4.5).

The remaining input to the limit calculation is the signal efficiency, obtained at intermediate values of m and Δm by linear 2-dimensional interpolation.

6 New Particle Search Results

We present limits on the pair production of charged scalar leptons, leptonically decaying charged Higgs bosons and charginos that decay to produce a charged lepton and invisible particles.

The 95% CL upper limit on new particle production at $\sqrt{s} = 189 \text{ GeV}$, obtained by combining the data at $\sqrt{s} = 189 \text{ GeV}$ and $\sqrt{s} = 183 \text{ GeV}$ is calculated at each kinematically allowed point on a 0.5 GeV by 0.5 GeV grid of m and Δm , using the L_R distributions for signal and

²Particle masses less than 45 GeV are not considered because these masses were accessible at LEP1 and because radiative return to the Z means that the event topology can be different.

background, the L_R values of the data events, and the efficiency of the general selection at that point as input.

In addition to the Monte Carlo statistical error on the signal efficiency, we assign a 10% systematic error on the estimated selection efficiency to take into account uncertainties in trigger efficiency, detector occupancy, lepton identification efficiency, luminosity measurement, the interpolation procedure, and deficiencies in the Monte Carlo generators and the detector simulation. An additional systematic error in the stau analysis is the effect of tau polarisation in the modelling of the stau signal. It is possible for the tau produced in stau decay to have any polarisation value in the range $[-1,1]$ [24]. This was studied by using stau Monte Carlo events with tau polarisations of $+1$, 0 and -1 to determine the amount by which the expected limit on the cross-section times branching ratio squared is overestimated or underestimated if a polarisation of zero is assumed when the true polarisation is $+1$ or -1 . The size of this effect was found to vary with m and Δm , but to be always less than about 5% , and so is included in the 10% systematic error.

At high values of Δm the dominant background to the searches for new physics results from W^+W^- production. High statistics Monte Carlo samples for this process are available that describe well the OPAL data [25]. In addition to the Monte Carlo statistical error, we assign a 10% systematic error on the estimated background to take into account uncertainties in the shapes of the L_R distributions and reference histograms, and in the interpolation procedure, and deficiencies in the Monte Carlo detector simulation. At low values of Δm the dominant background results from $e^+e^-\ell^+\ell^-$ events. The background uncertainty at low Δm is dominated by the limited Monte Carlo statistics; the uncertainty is typically 20–80% at low Δm . In setting limits the Monte Carlo statistical errors and other systematics are taken into account according to the method described in [26].

6.1 Limits on Production Cross-section Times Branching Ratio Squared

Limits on the production cross-section times branching ratio squared for new physics processes are now presented in a manner intended to minimise the number of model assumptions. The 95% CL upper limits at $\sqrt{s} = 189$ GeV shown in Figures 6 – 11 are obtained by combining the data at the two centre-of-mass energies 183 and 189 GeV using the assumption that the cross-section varies as β^3/s for sleptons and β/s for charginos. The chosen functional forms are used for simplicity in presenting the data and represent an approximation, particularly for processes in which t -channel exchange may be important, that is, selectron pair and chargino pair production. In these cases the cross-section dependence on centre-of-mass energy is model dependent, depending on the mass of the exchanged particles and the couplings of the neutralinos and charginos. The selectron Monte Carlo events were generated at $\mu = -200$ GeV and $\tan\beta = 1.5$ using SUSYGEN. We have found by varying μ and $\tan\beta$ that the above choice gives a conservative estimate of the selection efficiency for selectrons.

Upper limits at 95% CL on the selectron pair cross-section at $\sqrt{s} = 189$ GeV times branching ratio squared for the decay $\tilde{e}^- \rightarrow e^- \tilde{\chi}_1^0$ are shown in Figure 6 as a function of selectron mass and lightest neutralino mass. These limits are applicable to $\tilde{e}_L^+ \tilde{e}_L^-$ and $\tilde{e}_R^+ \tilde{e}_R^-$ production. The corresponding plots for the smuon and stau pair searches are shown in Figures 7 and 8, respectively. Note that if the LSP is the gravitino, \tilde{G} (effectively massless), then for prompt slepton decays to a lepton and a gravitino the experimental signature would be the same as

that for $\tilde{\ell}^- \rightarrow \ell^- \tilde{\chi}_1^0$ with a massless neutralino. In this case the limits given in Figures 6 – 8 for $m_{\tilde{\chi}_1^0} = 0$ may be interpreted as limits on the decay $\tilde{\ell}^- \rightarrow \ell^- \tilde{G}$

The upper limit at 95% CL on the chargino pair production cross-section times branching ratio squared for the decay $\tilde{\chi}_1^\pm \rightarrow \ell^\pm \tilde{\nu}_\ell$ (2-body decay) is shown in Figure 9. The limit has been calculated for the case where the three sneutrino generations are mass degenerate. The upper limit at 95% CL on the chargino pair production cross-section times branching ratio squared for the decay $\tilde{\chi}_1^\pm \rightarrow W^\pm \tilde{\chi}_1^0 \rightarrow \ell^\pm \nu \tilde{\chi}_1^0$ (3-body decay) is shown in Figure 10.

The upper limit at 95% CL on the charged Higgs boson pair production cross-section times branching ratio squared for the decay $H^\pm \rightarrow \tau^\pm \nu_\tau$ is shown as a function of m_{H^\pm} as the solid line in Figure 11. The limit is obtained by combining the 183 and 189 GeV data-sets assuming the m_{H^\pm} and \sqrt{s} dependence of the cross-section predicted by PYTHIA, which takes into account the effect of initial state radiation. The dashed line in Figure 11 shows the prediction from PYTHIA at $\sqrt{s} = 189$ GeV for a 100% branching ratio for the decay $H^\pm \rightarrow \tau^\pm \nu_\tau$. With this assumption we set a lower limit at 95% CL on m_{H^\pm} of 82.8 GeV.

6.2 Expected Limits and Confidence Levels for Consistency with Expectation

Table 3 gives the values of the following quantities for a number of values of m and Δm in the search for selectrons:

1. The signal selection efficiency of the general selection at 189 GeV (the efficiencies at 183 GeV are similar).
2. The 95% CL upper limit on the cross-section times branching ratio squared at 189 GeV, obtained by combining the data at $\sqrt{s} = 189$ GeV and $\sqrt{s} = 183$ GeV.
3. The expected 95% CL upper limit on the cross-section times branching ratio squared in the absence of signal $\langle \sigma_{95} \rangle$. This is calculated using an ensemble of 1000 toy Monte Carlo experiments to simulate the data, in which the total number of candidates for each experiment is drawn from a Poisson distribution with mean equal to the number of events expected from the Standard Model, and for each candidate, a value of L_R is assigned, chosen randomly according to the expected L_R distribution for Standard Model processes. The expected limit at a given point in m and Δm is the mean value of the limit for the ensemble of simulated experiments.
4. The confidence level for consistency with the Standard Model, calculated as the fraction of the simulated experiments for which the upper limit on the cross-section times branching ratio squared is greater than or equal to the value calculated using the actual data. In the absence of signal, a CL of 50% is expected on average ³.

Tables 4, 5, 6, 7 and 8 show the same information for smuons, staus, charginos with two-body decay, charginos with three-body decay and charged Higgs, respectively.

³Values of 100% correspond to points where there are no candidate events with non-zero L_R in the OPAL data. In this case, all toy Monte Carlo experiments will have a value of σ_{95} equal to or (if there are candidates with non-zero L_R) greater than the value for the actual data.

For some points in m and Δm in Tables 3 and 4, the confidence level for consistency with the Standard Model is small (around 1%). The probability of getting a low confidence level for one or more points in m and Δm for one or more of the search channels depends on the degree of correlation among the different $(m, \Delta m)$ points and among the different channels. The degree of correlations between adjacent points is strong when the momentum distributions for those points are similar. The momentum distributions vary slowly with both m and Δm when Δm is high (hence the clustering of low confidence level values in Table 4), but vary considerably with Δm when Δm is low.

This effect was investigated by calculating the cross-section limits for each of 1000 experiments in which the data is simulated by randomly selected Standard Model Monte Carlo events. For each experiment, the number of events taken from a Monte Carlo sample simulating a given process is drawn from a Poisson distribution with mean equal to the number of events expected for that process. For each experiment, the confidence level at each $(m, \Delta m)$ point at which signal Monte Carlo has been generated was calculated as already described, and the number of experiments for which a confidence level of 0.6%⁴ or less is obtained for at least one point in m and Δm in at least one search channel was determined. This was found to be the case for 390 of the 1000 experiments.

As a cross-check, taking the mean of the ensemble of limits obtained at each $(m, \Delta m)$ point for these simulated experiments was used as an alternative to the method described above to obtain $\langle\sigma_{95}\rangle$. The results were found to be consistent.

6.3 Limits on New Particle Masses

We can use our data to set limits on the masses of right-handed sleptons⁵ based on the expected right-handed slepton pair cross-sections and branching ratios. The cross-sections have been calculated using SUSYGEN at each centre-of-mass energy and take into account initial state radiation. In Figure 12 we show limits on right-handed smuons as a function of smuon mass and lightest neutralino mass for several assumed values of the branching ratio squared for $\tilde{\mu}_R^\pm \rightarrow \mu^\pm \tilde{\chi}_1^0$. The expected limit, calculated using Monte Carlo only, for a branching ratio of 100% is also shown. For a branching ratio $\tilde{\mu}_R^\pm \rightarrow \mu^\pm \tilde{\chi}_1^0$ of 100% and for a smuon-neutralino mass difference exceeding 3 GeV, right-handed smuons are excluded at 95% CL for masses below 82.3 GeV. The 95% CL upper limit on the production of right-handed $\tilde{\tau}^+ \tilde{\tau}^-$ times the branching ratio squared for $\tilde{\tau}_R^\pm \rightarrow \tau^\pm \tilde{\chi}_1^0$ is shown in Figure 13. The expected limit for a branching ratio of 100% is also shown. For a branching ratio $\tilde{\tau}_R^\pm \rightarrow \tau^\pm \tilde{\chi}_1^0$ of 100% and for a stau-neutralino mass difference exceeding 8 GeV, right-handed staus are excluded at 95% CL for masses below 81.0 GeV. No mixing between $\tilde{\tau}_L$ and $\tilde{\tau}_R$ is assumed. However, the cross-section ratio $\sigma_{\tilde{\tau}_1^+ \tilde{\tau}_1^-} / \sigma_{\tilde{\tau}_R^+ \tilde{\tau}_R^-}$ at $\sqrt{s}=189$ GeV varies between 0.89 and 1.20, depending only on the mixing angle. Using this information, the limits shown in Figure 13 can be applied to any degree of stau mixing by multiplying the predicted cross-section for $\tilde{\tau}_R^+ \tilde{\tau}_R^-$ by the value of $\sigma_{\tilde{\tau}_1^+ \tilde{\tau}_1^-} / \sigma_{\tilde{\tau}_R^+ \tilde{\tau}_R^-}$ corresponding to the mixing angle considered. The hatched region in Figure 13 shows the range of possible positions of the line defining the excluded region for a branching ratio $\tilde{\tau}_1^\pm \rightarrow \tau^\pm \tilde{\chi}_1^0$ of 100% for any degree of stau mixing.

⁴This is the lowest value of the confidence level in Tables 3 to 8.

⁵ The right-handed slepton is expected to be lighter than the left-handed slepton. The right-handed one tends (not generally valid for selectrons) to have a lower pair production cross-section, and so conventionally limits are given for this (usually) conservative case.

For the case of a massless neutralino (or gravitino) and 100% branching ratio, right-handed smuons and staus are excluded at 95% CL for masses below 85.4 GeV and 81.1 GeV, respectively, and $\tilde{\tau}_1^\pm$ is excluded at 95% CL for masses below 80.0 GeV, for any degree of stau mixing.

An alternative approach is to set limits taking into account the predicted cross-section and branching ratio for specific choices of the parameters within the Minimal Supersymmetric Standard Model (MSSM)⁶. For $\mu < -100$ GeV and for two values of $\tan\beta$ (1.5 and 35), Figures 14, 15 and 16 show 95% CL exclusion regions in the $(m_{\tilde{\ell}_R^\pm}, m_{\tilde{\chi}_1^0})$ plane for right-handed selectrons, smuons and staus, respectively. For $\mu < -100$ GeV and $\tan\beta = 1.5$, right-handed sleptons are excluded at 95% CL as follows: selectrons with masses below 87.1 GeV for $m_{\tilde{e}^-} - m_{\tilde{\chi}_1^0} > 5$ GeV; smuons with masses below 81.7 GeV for $m_{\tilde{\mu}^-} - m_{\tilde{\chi}_1^0} > 3$ GeV; and staus with masses below 75.9 GeV for $m_{\tilde{\tau}^-} - m_{\tilde{\chi}_1^0} > 7$ GeV.

7 Summary and Conclusions

A selection of di-lepton events with significant missing transverse momentum is performed using a total data sample of 237.4 pb^{-1} at e^+e^- centre-of-mass energies of 183 and 189 GeV. The observed numbers of events, 78 at 183 GeV and 301 at 189 GeV, are consistent with the numbers expected from Standard Model processes, dominantly arising from W^+W^- production with each W decaying leptonically.

Further discrimination techniques are employed to search for the pair production of charged scalar leptons, leptonically decaying charged Higgs bosons and charginos that decay to produce a charged lepton and invisible particles. No evidence for new phenomena is apparent and model independent limits on the production cross-section times branching ratio squared for each new physics process are presented.

Assuming a 100% branching ratio for the decay $\tilde{\ell}_R^\pm \rightarrow \ell^\pm \tilde{\chi}_1^0$, we exclude at 95% CL: right-handed smuons with masses below 82.3 GeV for $m_{\tilde{\mu}^-} - m_{\tilde{\chi}_1^0} > 3$ GeV and right-handed staus with masses below 81.0 GeV for $m_{\tilde{\tau}^-} - m_{\tilde{\chi}_1^0} > 8$ GeV. Right-handed selectrons are excluded at 95% CL for masses below 87.1 GeV for $m_{\tilde{e}^-} - m_{\tilde{\chi}_1^0} > 5$ GeV within the framework of the MSSM assuming $\mu < -100$ GeV and $\tan\beta = 1.5$. Charged Higgs bosons are excluded at 95% CL for masses below 82.8 GeV, assuming a 100% branching ratio for the decay $H^\pm \rightarrow \tau^\pm \nu_\tau$.

The cross-section times branching ratio squared limits from the selectron, smuon and two-body chargino searches presented here are used in the interpretation of the results of [27] in terms of mass limits on charginos and neutralinos.

Acknowledgements.

We particularly wish to thank the SL Division for the efficient operation of the LEP accelerator at all energies and for their continuing close cooperation with our experimental group. We thank our colleagues from CEA, DAPNIA/SPP, CE-Saclay for their efforts over the years on the time-of-flight and trigger systems which we continue to use. In addition to the support staff

⁶ In particular regions of the MSSM parameter space, the branching ratio for $\tilde{\ell}^\pm \rightarrow \ell^\pm \tilde{\chi}_1^0$ can be essentially zero and so it is not possible to provide general limits on sleptons within the MSSM on the basis of this search alone. The predicted cross-sections and branching ratios within the MSSM are obtained using SUSYGEN and are calculated with the gauge unification relation, $M_1 = \frac{5}{3} \tan^2 \theta_W M_2$.

at our own institutions we are pleased to acknowledge the
Department of Energy, USA,
National Science Foundation, USA,
Particle Physics and Astronomy Research Council, UK,
Natural Sciences and Engineering Research Council, Canada,
Israel Science Foundation, administered by the Israel Academy of Science and Humanities,
Minerva Gesellschaft,
Benozio Center for High Energy Physics,
Japanese Ministry of Education, Science and Culture (the Monbusho) and a grant under the
Monbusho International Science Research Program,
Japanese Society for the Promotion of Science (JSPS),
German Israeli Bi-national Science Foundation (GIF),
Bundesministerium für Bildung, Wissenschaft, Forschung und Technologie, Germany,
National Research Council of Canada,
Research Corporation, USA,
Hungarian Foundation for Scientific Research, OTKA T-029328, T023793 and OTKA F-023259.

References

- [1] H.P. Nilles, Phys. Rep. **110** (1984) 1;
H.E. Haber and G.L. Kane, Phys. Rep. **117** (1985).
- [2] OPAL Collab., K. Ackerstaff *et al.*, Eur. Phys. J. **C4** (1998) 47.
- [3] OPAL Collab., “Search for Acoplanar Lepton Pair Events at $\sqrt{s} = 161, 172$ and 183 GeV”,
CERN-EP/98-122 (1998), accepted by Eur. Phys. J. **C**.
- [4] ALEPH Collaboration, R. Barate *et al.*, Phys. Lett. **B433** (1998) 176.
DELPHI Collaboration, P. Abreu *et al.*, Eur. Phys. J. **C6** (1999) 385.
L3 Collaboration, M. Acciarri *et al.*, Eur. Phys. J. **C4** (1998) 207.
- [5] OPAL Collab., K. Ahmet *et al.*, Nucl. Instr. Meth. **A305** (1991) 275;
S. Anderson, Nucl. Instr. Meth. **A403** (1998) 326.
- [6] G. Aguillion *et al.*, Nucl. Instr. Meth. **A417** (1998) 266.
- [7] grc4f 1.0 generator: J. Fujimoto *et al.*, Comp. Phys. Comm. **100** (1997) 128;
J. Fujimoto *et al.*, in *Physics at LEP2*, edited by G. Altarelli, T. Sjöstrand and F. Zwirner,
CERN 96-01, Vol. 2 (1996) p. 30.
- [8] S. Jadach *et al.*, “Monte Carlo program KORALW 1.42 for All Four-Fermion Final States
in e^+e^- Collision”, CERN-TH/98-242 (1998).
- [9] EXCALIBUR generator: F.A. Berends, R. Pittau, R. Kleiss, Comp. Phys. Comm. **85** (1995)
437.
- [10] J.A.M. Vermaseren, Nucl. Phys. **B229** (1983) 347.

- [11] PHOJET 1.05 generator: E. Budinov *et al.*, in *Physics at LEP2*, edited by G. Altarelli, T. Sjöstrand and F. Zwirner, CERN 96-01, Vol. 2 (1996) p. 216; R. Engel and J. Ranft, Phys. Rev. **D54** (1996) 4244.
- [12] G. Marchesini *et al.*, Comp. Phys. Comm. **67** (1992) 465.
- [13] BHWIDE generator: S. Jadach, W. Płaczek, B.F.L. Ward, Phys. Lett. **390** (1997) 298.
- [14] TEEGG generator: D. Karlen, Nucl. Phys. **B289** (1987) 23.
- [15] KORALZ 4.0 generator: S. Jadach, B.F.L. Ward, Z. Wąs, Comp. Phys. Comm. **79** (1994) 503.
- [16] PYTHIA 5.721 and JETSET 7.408 generators: T. Sjöstrand, Comp. Phys. Comm. **82** (1994) 74; LU TP 95-20.
- [17] NUNUGPV98 generator: G. Montagna, M. Moretti, O. Nicrosini and F. Piccinini, CERN-TH/98-238.
- [18] SUSYGEN generator: S. Katsanevas and S. Melachroinos, in *Physics at LEP2*, edited by G. Altarelli, T. Sjöstrand and F. Zwirner, CERN 96-01, Vol. 2 (1996) p. 216. S. Katsanevas and P. Morawitz, Comp. Phys. Comm. **112** (1998) 227.
- [19] DFGT generator: C. Dionisi *et al.*, in “*Physics at LEP2*”, edited by G. Altarelli, T. Sjöstrand and F. Zwirner, CERN 96-01, Vol. 2 (1996) p. 337.
- [20] HZHA generator: P. Janot, in “*Physics at LEP2*”, edited by G. Altarelli, T. Sjöstrand and F. Zwirner, CERN 96-01, Vol. 2 (1996) p. 309.
- [21] J. Allison *et al.*, Nucl. Instr. Meth. **A317** (1992) 47.
- [22] J. Allison, Comp. Phys. Comm. **77** (1993) 377.
- [23] A.G. Frodesen, O. Skjeggstad, and H. Tøfte, “*Probability and Statistics in Particle Physics*”, Universitetsforlaget, 1979, ISBN 82-00-01-01906-3; S.L. Meyer, “*Data Analysis for Scientists and Engineers*”, John Wiley and Sons, 1975, ISBN 0-471-59995-6.
- [24] M.M. Nojiri, Phys. Rev. **D51** (1995) 6281.
- [25] OPAL Collab., G. Abbiendi *et al.*, Eur. Phys. J. **C8** (1999) 191.
- [26] R.D. Cousins and V.L. Highland, Nucl. Instr. Meth. **A320** (1992) 331.
- [27] OPAL Collab., G. Abbiendi *et al.*, “Search for Chargino and Neutralino Production at $\sqrt{s} = 189\text{GeV}$ at LEP”, CERN-EP/99-xxx, to be submitted to Phys. Lett. B.

Δm (GeV)	$m_{\tilde{e}^-}$ (GeV)					
	45	55	65	75	85	94
signal selection efficiency of the general selection at 189 GeV (%)						
2	13.0±1.1	10.5±1.0	7.8±0.8	4.2±0.6	1.4±0.4	0.4±0.2
2.5	25.1±1.4	21.4±1.3	22.1±1.3	18.5±1.2	12.9±1.1	7.4±0.8
5	56.6±1.6	59.5±1.6	59.0±1.6	60.5±1.5	60.2±1.5	55.9±1.6
10	71.0±1.4	74.4±1.4	76.7±1.3	76.3±1.3	77.5±1.3	76.0±1.4
20	78.8±1.3	81.6±1.2	85.2±1.1	85.2±1.1	84.6±1.1	85.9±1.1
$m/2$	78.5±1.3	84.8±1.1	87.4±1.0	90.6±0.9	90.4±0.9	92.1±0.9
$m-20$	79.0±1.3	85.6±1.1	88.8±1.0	90.4±0.9	91.8±0.9	93.1±0.8
$m-10$	78.9±1.3	84.9±1.1	89.3±1.0	90.3±0.9	91.1±0.9	92.5±0.8
m	77.4±1.3	84.1±1.2	88.7±1.0	90.1±0.9	91.3±0.9	93.2±0.8
95% CL upper limit on the cross-section times $BR^2(\tilde{e} \rightarrow e\tilde{\chi}_1^0)$ (fb)						
2	93.8	117.2	164.8	305.5	973.8	4138.6
2.5	49.2	56.5	56.1	67.7	106.1	223.7
5	36.7	25.7	24.3	21.9	23.3	29.6
10	63.1	50.2	43.8	30.8	26.8	22.0
20	64.8	50.9	44.7	48.9	54.7	25.6
$m/2$	92.3	73.2	79.4	54.5	35.3	20.0
$m-20$	97.8	101.5	93.3	87.8	63.4	23.5
$m-10$	91.5	76.9	73.8	89.9	70.4	29.6
m	81.4	84.6	85.8	86.8	64.0	34.5
expected upper limit on the cross-section times $BR^2(\tilde{e} \rightarrow e\tilde{\chi}_1^0)$ (fb)						
2	148.3	175.1	237.0	414.5	1325.7	4616.9
2.5	82.0	90.9	87.4	104.9	136.6	264.2
5	42.2	39.3	38.9	34.6	33.8	34.1
10	40.4	33.3	28.5	25.8	24.5	24.8
20	69.1	52.8	43.2	34.8	27.9	23.6
$m/2$	76.1	71.5	62.5	62.0	57.2	33.6
$m-20$	80.7	78.7	79.3	80.0	70.3	38.9
$m-10$	84.9	78.6	79.6	81.1	69.3	37.9
m	81.9	76.0	76.0	80.8	71.1	38.8
CL for consistency with SM (%)						
2	100.0	100.0	100.0	100.0	100.0	100.0
2.5	100.0	100.0	100.0	100.0	100.0	100.0
5	57.0	88.6	90.5	95.4	89.1	100.0
10	5.2	6.8	6.3	18.0	33.1	83.9
20	47.6	44.6	38.2	10.4	0.6	19.7
$m/2$	20.7	37.7	17.9	53.6	88.8	99.9
$m-20$	20.3	14.4	22.8	27.8	52.0	95.0
$m-10$	30.5	43.2	45.6	27.4	37.2	72.3
m	38.2	28.1	24.9	30.9	51.2	56.0

Table 3: Signal selection efficiency of the general selection at 189 GeV, 95% CL upper limit on the cross-section times $BR^2(\tilde{e} \rightarrow e\tilde{\chi}_1^0)$, expected upper limit on the cross-section times $BR^2(\tilde{e} \rightarrow e\tilde{\chi}_1^0)$, and the confidence level for consistency with the Standard Model in the search for $\tilde{e}^+\tilde{e}^-$ production for different values of $m_{\tilde{e}^-}$ and Δm .

Δm (GeV)	$m_{\tilde{\mu}^-}$ (GeV)					
	45	55	65	75	85	94
signal selection efficiency of the general selection at 189 GeV (%)						
2	14.9±1.1	14.1±1.1	9.8±0.9	6.5±0.8	0.7±0.3	0.0±0.0
2.5	26.7±1.4	27.7±1.4	25.0±1.4	21.3±1.3	14.3±1.1	8.0±0.9
5	58.7±1.6	60.5±1.5	60.4±1.5	60.0±1.5	60.3±1.5	57.4±1.6
10	75.8±1.4	76.7±1.3	76.2±1.3	76.4±1.3	76.5±1.3	74.1±1.4
20	85.4±1.1	86.0±1.1	84.8±1.1	84.2±1.2	84.0±1.2	83.2±1.2
$m/2$	86.3±1.1	87.8±1.0	87.2±1.1	90.4±0.9	90.4±0.9	91.7±0.9
$m-20$	86.7±1.1	89.2±1.0	89.7±1.0	91.2±0.9	92.9±0.8	92.8±0.8
$m-10$	88.5±1.0	90.6±0.9	89.6±1.0	91.3±0.9	92.4±0.8	93.0±0.8
m	88.6±1.0	90.6±0.9	89.8±1.0	91.1±0.9	92.1±0.9	92.5±0.8
95% CL upper limit on the cross-section times $BR^2(\tilde{\mu} \rightarrow \mu\tilde{\chi}_1^0)$ (fb)						
2	105.6	119.3	177.3	300.8	2069.3	–
2.5	63.3	61.5	72.0	88.8	98.8	206.9
5	30.3	31.0	39.5	31.8	34.1	28.8
10	35.0	22.7	18.5	17.3	18.2	22.3
20	53.5	38.7	39.9	41.3	37.6	25.5
$m/2$	64.7	76.7	81.6	71.1	51.7	44.1
$m-20$	80.1	100.5	104.6	89.6	45.3	34.3
$m-10$	85.4	94.6	92.8	62.9	43.4	34.3
m	83.5	87.7	88.8	58.9	43.5	34.7
expected upper limit on the cross-section times $BR^2(\tilde{\mu} \rightarrow \mu\tilde{\chi}_1^0)$ (fb)						
2	112.8	116.1	169.0	286.8	2977.5	–
2.5	67.6	64.7	68.9	82.4	119.5	226.1
5	34.8	33.8	31.2	28.2	28.8	30.2
10	30.8	27.4	25.3	22.6	22.6	24.3
20	47.5	39.3	35.9	31.3	25.3	22.1
$m/2$	50.9	50.9	50.4	51.0	50.1	33.4
$m-20$	51.8	52.8	55.8	58.7	56.8	36.4
$m-10$	53.1	51.1	53.7	56.5	56.5	38.1
m	50.6	49.7	52.9	57.6	56.7	39.5
CL for consistency with SM (%)						
2	64.6	47.9	45.7	43.7	100.0	–
2.5	65.7	60.6	54.1	40.2	100.0	100.0
5	57.8	47.5	19.0	35.9	27.2	100.0
10	26.1	63.8	76.1	100.0	100.0	100.0
20	27.8	42.1	30.0	15.0	7.5	8.5
$m/2$	17.6	7.6	4.8	10.6	36.0	14.2
$m-20$	6.3	1.7	1.1	6.1	66.8	49.0
$m-10$	4.4	1.3	2.7	29.1	69.0	52.3
m	3.4	2.8	3.9	36.3	71.3	57.1

Table 4: Signal selection efficiency of the general selection at 189 GeV, 95% CL upper limit on the cross-section times $BR^2(\tilde{\mu} \rightarrow \mu\tilde{\chi}_1^0)$, expected upper limit on the cross-section times $BR^2(\tilde{\mu} \rightarrow \mu\tilde{\chi}_1^0)$, and the confidence level for consistency with the Standard Model in the search for $\tilde{\mu}^+\tilde{\mu}^-$ production for different values of $m_{\tilde{\mu}^-}$ and Δm .

Δm (GeV)	$m_{\tilde{\tau}^-}$ (GeV)					
	45	55	65	75	85	94
signal selection efficiency of the general selection at 189 GeV (%)						
2	0.2±0.0	0.1±0.0	0.1±0.0	0.0±0.0	0.0±0.0	0.0±0.0
2.5	0.7±0.1	0.5±0.1	0.3±0.0	0.3±0.0	0.1±0.0	0.0±0.0
5	15.6±0.3	14.0±0.3	13.1±0.3	11.6±0.3	10.3±0.3	9.1±0.3
10	38.3±0.4	39.1±0.4	39.5±0.4	38.8±0.4	39.4±0.4	38.8±0.4
20	57.4±0.4	59.4±0.4	59.9±0.4	60.9±0.4	60.9±0.4	62.2±0.4
$m/2$	59.3±0.4	64.8±0.4	69.6±0.4	71.8±0.4	73.7±0.4	74.5±0.4
$m-20$	60.6±0.4	69.1±0.4	73.4±0.4	74.4±0.4	77.5±0.4	78.3±0.4
$m-10$	65.2±0.4	71.1±0.4	73.9±0.4	76.2±0.4	77.7±0.4	79.2±0.4
m	66.2±0.4	71.3±0.4	74.5±0.4	76.1±0.4	77.7±0.4	79.0±0.4
95% CL upper limit on the cross-section times $BR^2(\tilde{\tau} \rightarrow \tau\tilde{\chi}_1^0)$ (fb)						
2	12180.7	32560.6	16554.6	–	–	–
2.5	2678.7	4145.1	5526.8	6808.6	19454.0	–
5	137.6	168.4	181.7	243.9	274.5	324.1
10	106.8	92.1	81.5	75.7	74.2	86.7
20	101.1	92.8	84.7	86.5	77.1	59.2
$m/2$	100.8	97.5	87.4	76.3	76.2	90.6
$m-20$	106.4	93.5	78.7	75.8	76.0	87.6
$m-10$	119.8	97.1	83.2	75.5	73.7	97.6
m	115.4	94.1	86.1	76.6	81.3	87.6
expected upper limit on the cross-section times $BR^2(\tilde{\tau} \rightarrow \tau\tilde{\chi}_1^0)$ (fb)						
2	11163.9	20013.4	19897.3	–	–	–
2.5	2916.5	4380.8	6850.2	7709.0	17774.8	–
5	189.5	209.3	221.8	237.2	262.6	284.6
10	107.0	103.4	97.4	98.2	94.2	92.1
20	103.4	95.8	89.7	82.9	79.1	74.3
$m/2$	106.9	104.7	99.5	95.1	93.8	96.1
$m-20$	108.3	107.1	108.3	107.5	108.1	112.2
$m-10$	113.9	112.1	114.4	109.7	114.4	111.6
m	118.2	114.1	112.4	110.6	113.7	114.0
CL for consistency with SM (%)						
2	37.4	7.4	100.0	–	–	–
2.5	56.8	41.2	77.2	65.5	45.3	–
5	75.5	66.6	62.8	38.6	32.8	23.0
10	40.7	56.8	61.3	70.0	66.6	50.3
20	43.5	44.0	46.9	37.7	42.5	67.2
$m/2$	46.1	47.5	54.7	64.4	64.1	47.5
$m-20$	41.4	54.3	74.1	76.0	75.0	67.0
$m-10$	33.0	56.0	72.9	79.0	83.2	54.0
m	40.6	59.7	67.4	79.0	73.3	69.6

Table 5: Signal selection efficiency of the general selection at 189 GeV, 95% CL upper limit on the cross-section times $BR^2(\tilde{\tau} \rightarrow \tau\tilde{\chi}_1^0)$, expected upper limit on the cross-section times $BR^2(\tilde{\tau} \rightarrow \tau\tilde{\chi}_1^0)$, and the confidence level for consistency with the Standard Model in the search for $\tilde{\tau}^+\tilde{\tau}^-$ production for different values of $m_{\tilde{\tau}^-}$ and Δm .

Δm (GeV)	$m_{\tilde{\chi}_1^\pm}$ (GeV)					
	50	60	70	80	90	94
signal selection efficiency of the general selection at 189 GeV (%)						
2	7.9±0.4	6.6±0.4	4.9±0.3	2.3±0.2	0.5±0.1	0.1±0.0
3	21.6±0.7	21.6±0.7	20.6±0.6	19.5±0.6	15.8±0.6	13.3±0.5
4	34.3±0.8	33.5±0.7	33.7±0.7	33.6±0.7	31.5±0.7	32.5±0.7
5	41.3±0.8	43.4±0.8	42.5±0.8	41.9±0.8	43.0±0.8	44.7±0.8
10	61.0±0.8	64.4±0.8	63.6±0.8	63.9±0.8	63.5±0.8	65.4±0.8
20	–	75.8±0.7	77.4±0.7	78.2±0.7	79.5±0.6	78.3±0.7
$(m - 15)/2$	–	77.1±0.7	82.2±0.6	82.7±0.6	85.8±0.6	86.6±0.5
$m - 35$	69.7±0.7	78.3±0.7	83.2±0.6	85.9±0.6	87.4±0.5	89.0±0.5
95% CL upper limit on the cross-section times $BR^2(\tilde{\chi}_1^\pm \rightarrow \ell^\pm \tilde{\nu})$ (fb)						
2	241.3	262.3	330.0	755.6	3368.0	20947.5
3	103.8	89.2	98.6	103.8	88.6	125.3
4	62.3	60.7	68.3	61.5	80.1	54.7
5	53.0	44.9	58.5	50.3	63.6	62.5
10	92.2	82.4	57.7	39.0	39.4	38.2
20	–	72.1	64.8	60.8	65.3	40.8
$(m - 15)/2$	–	81.9	83.9	88.2	61.5	53.7
$m - 35$	84.6	87.0	116.9	118.5	70.1	42.6
expected upper limit on the cross-section times $BR^2(\tilde{\chi}_1^\pm \rightarrow \ell^\pm \tilde{\nu})$ (fb)						
2	289.4	313.9	387.6	900.9	4055.8	22119.2
3	123.1	117.9	108.4	119.4	134.2	165.3
4	86.7	82.2	75.4	70.9	77.4	73.1
5	77.5	68.4	68.7	64.7	59.0	60.1
10	79.5	64.0	58.2	52.1	47.8	44.3
20	–	108.5	84.7	68.2	49.7	38.7
$(m - 15)/2$	–	121.0	119.0	115.5	108.3	74.7
$m - 35$	103.8	130.8	154.0	166.4	143.7	88.8
CL for consistency with SM (%)						
2	63.3	59.1	68.3	70.7	76.5	66.1
3	61.4	72.3	48.1	56.9	100.0	73.5
4	80.1	77.6	51.8	53.4	36.9	70.2
5	82.9	88.6	59.0	72.0	33.5	29.5
10	24.8	14.7	42.1	76.4	64.2	59.2
20	–	80.9	70.0	53.1	15.2	33.6
$(m - 15)/2$	–	79.5	76.0	69.4	93.4	79.0
$m - 35$	63.9	81.4	63.6	72.7	97.0	98.9

Table 6: Signal selection efficiency of the general selection at 189 GeV, 95% CL upper limit on the cross-section times $BR^2(\tilde{\chi}_1^\pm \rightarrow \ell^\pm \tilde{\nu})$, expected upper limit on the cross-section times $BR^2(\tilde{\chi}_1^\pm \rightarrow \ell^\pm \tilde{\nu})$, and the confidence level for consistency with the Standard Model in the search for $\tilde{\chi}_1^+ \tilde{\chi}_1^-$ (2-body decays) production for different values of $m_{\tilde{\chi}_1^\pm}$ and Δm . The bins without entries correspond to values of $m_{\tilde{\nu}} < 35$, which are excluded and therefore not considered in the analysis.

Δm (GeV)	$m_{\tilde{\chi}_1^\pm}$ (GeV)					
	50	60	70	80	90	94
signal selection efficiency of the general selection at 189 GeV (%)						
3	3.7±0.3	3.2±0.3	2.5±0.2	1.0±0.2	0.2±0.1	0.2±0.1
5	17.1±0.6	16.3±0.6	15.2±0.6	13.3±0.5	11.4±0.5	10.8±0.5
10	39.9±0.8	40.8±0.8	40.9±0.8	41.6±0.8	40.8±0.8	41.6±0.8
20	59.1±0.8	60.4±0.8	62.2±0.8	60.8±0.8	62.8±0.8	63.8±0.8
$m/2$	63.3±0.8	68.7±0.7	74.3±0.7	77.9±0.7	79.3±0.6	80.3±0.6
$m - 20$	67.3±0.7	72.6±0.7	78.0±0.7	81.2±0.6	83.9±0.6	84.0±0.6
$m - 10$	70.1±0.7	75.9±0.7	79.4±0.6	83.0±0.6	87.0±0.5	88.1±0.5
m	73.2±0.7	77.4±0.7	81.2±0.6	85.2±0.6	88.1±0.5	89.5±0.5
95% CL upper limit on the cross-section times $BR^2(\tilde{\chi}_1^\pm \rightarrow \ell^\pm \nu \tilde{\chi}_1^0)$ (fb)						
3	355.9	540.9	598.9	1578.0	5613.2	11457.9
5	111.0	116.1	134.6	114.5	156.9	272.9
10	74.7	60.4	66.5	61.0	56.2	65.5
20	91.3	78.4	68.0	64.3	51.0	52.8
$m/2$	105.8	99.7	82.9	69.9	88.0	121.6
$m - 20$	118.5	85.2	91.4	91.8	89.2	89.4
$m - 10$	111.6	103.7	104.2	101.6	88.1	60.6
m	133.7	132.4	117.3	117.2	99.6	57.6
expected upper limit on the cross-section times $BR^2(\tilde{\chi}_1^\pm \rightarrow \ell^\pm \nu \tilde{\chi}_1^0)$ (fb)						
3	563.5	668.8	791.2	2050.1	8303.3	10493.8
5	163.4	154.9	165.4	169.6	203.6	222.4
10	90.4	82.6	80.5	76.1	76.4	74.4
20	92.0	81.2	70.0	67.3	63.0	61.7
$m/2$	100.3	94.4	89.9	81.2	78.5	82.5
$m - 20$	103.7	114.8	114.9	113.9	131.0	140.5
$m - 10$	128.2	130.9	135.3	136.9	166.9	136.5
m	139.1	144.8	154.9	183.3	179.4	133.9
CL for consistency with SM (%)						
3	94.9	62.7	83.3	76.7	100.0	37.5
5	82.9	72.6	62.5	88.5	79.9	30.5
10	62.1	76.4	62.6	68.0	74.8	53.0
20	41.3	44.3	43.7	46.3	65.2	60.2
$m/2$	35.7	35.7	49.8	54.9	28.6	8.4
$m - 20$	26.7	69.0	65.0	62.3	80.5	84.9
$m - 10$	52.9	63.4	66.8	69.9	94.2	99.0
m	40.9	43.9	64.9	78.6	89.8	99.0

Table 7: Signal selection efficiency of the general selection at 189 GeV, 95% CL upper limit on the cross-section times $BR^2(\tilde{\chi}_1^\pm \rightarrow \ell^\pm \nu \tilde{\chi}_1^0)$, expected upper limit on the cross-section times $BR^2(\tilde{\chi}_1^\pm \rightarrow \ell^\pm \nu \tilde{\chi}_1^0)$, and the confidence level for consistency with the Standard Model in the search for $\tilde{\chi}_1^+ \tilde{\chi}_1^-$ (3-body decays) production for different values of $m_{\tilde{\chi}_1^\pm}$ and Δm .

m_{H^+} (GeV)					
45	55	65	75	85	94
signal selection efficiency of the general selection at 189 GeV (%)					
66.6±0.7	72.3±0.7	74.6±0.7	76.9±0.7	77.6±0.7	79.7±0.6
95% CL upper limit on the cross-section times $BR^2(H^\pm \rightarrow \tau^\pm \nu_\tau)$ (fb)					
113.6	84.8	81.5	73.2	77.0	80.1
expected upper limit on the cross-section times $BR^2(H^\pm \rightarrow \tau^\pm \nu_\tau)$ (fb)					
117.7	113.2	114.0	114.0	112.3	111.4
CL for consistency with SM (%)					
40.8	70.3	75.0	83.5	78.7	76.8

Table 8: Signal selection efficiency of the general selection at 189 GeV, 95% CL upper limit on the cross-section times $BR^2(H^\pm \rightarrow \tau^\pm \nu_\tau)$, expected upper limit on the cross-section times $BR^2(H^\pm \rightarrow \tau^\pm \nu_\tau)$, and the confidence level for consistency with the Standard Model in the search for H^+H^- production for different values of m_{H^+} .

OPAL

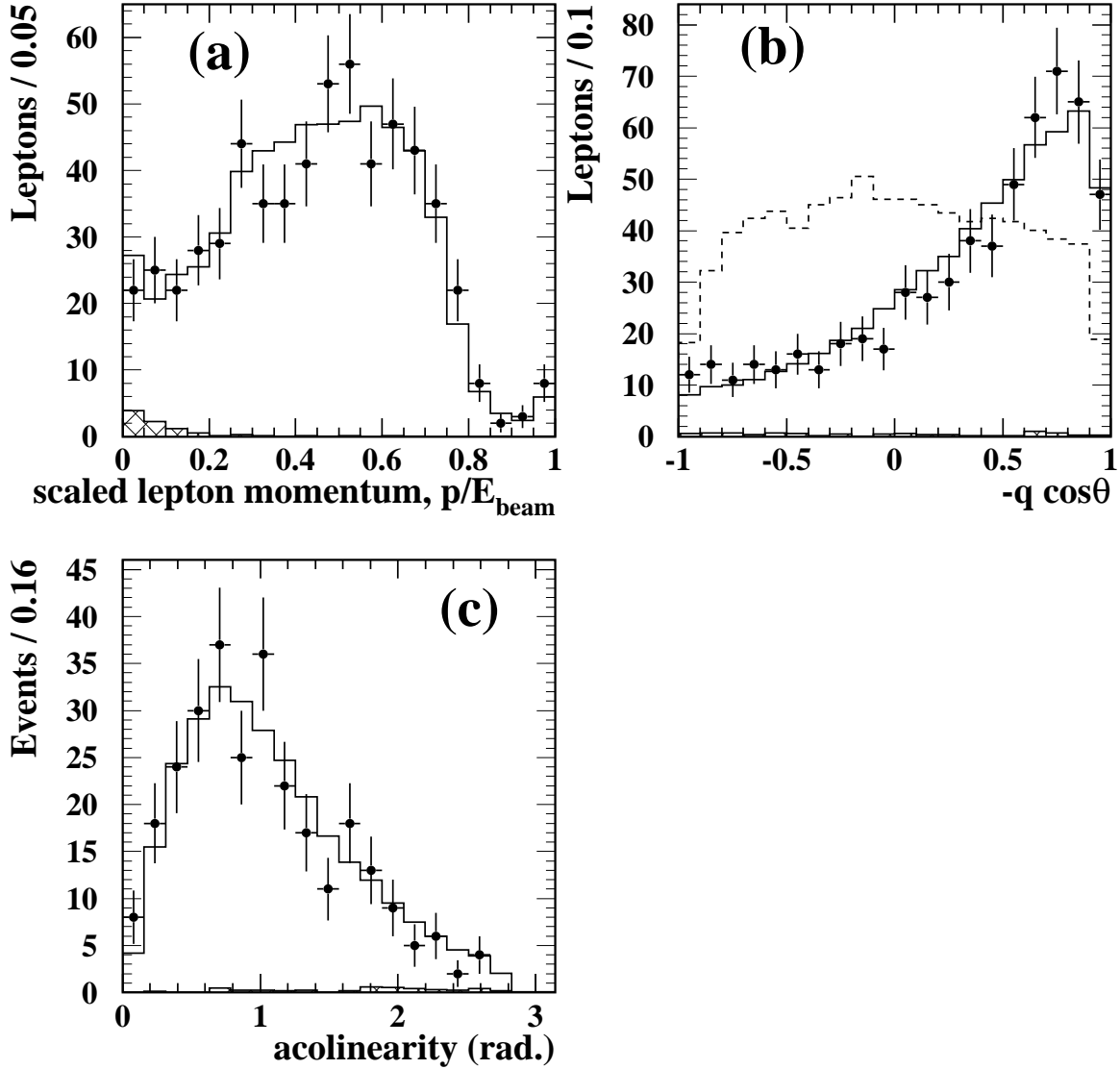


Figure 1: Distributions of (a) the lepton momentum divided by the beam energy, (b) $-q \cos \theta$ and (c) acolinearity (in radians), for the event sample produced by the general selection at $\sqrt{s} = 189$ GeV. The data are shown as the points with error bars. The Monte Carlo prediction for 4-fermion processes with genuine prompt missing energy and momentum ($\ell^+\nu\ell^-\bar{\nu}$) is shown as the open histogram and the background, arising mainly from processes with four charged leptons in the final state, is shown as the shaded histogram. In (b) the dashed histogram corresponds to the distribution expected from smuon pair production, with arbitrary normalisation. In (a) and (b) there are two entries per event for events containing two identified leptons.

OPAL

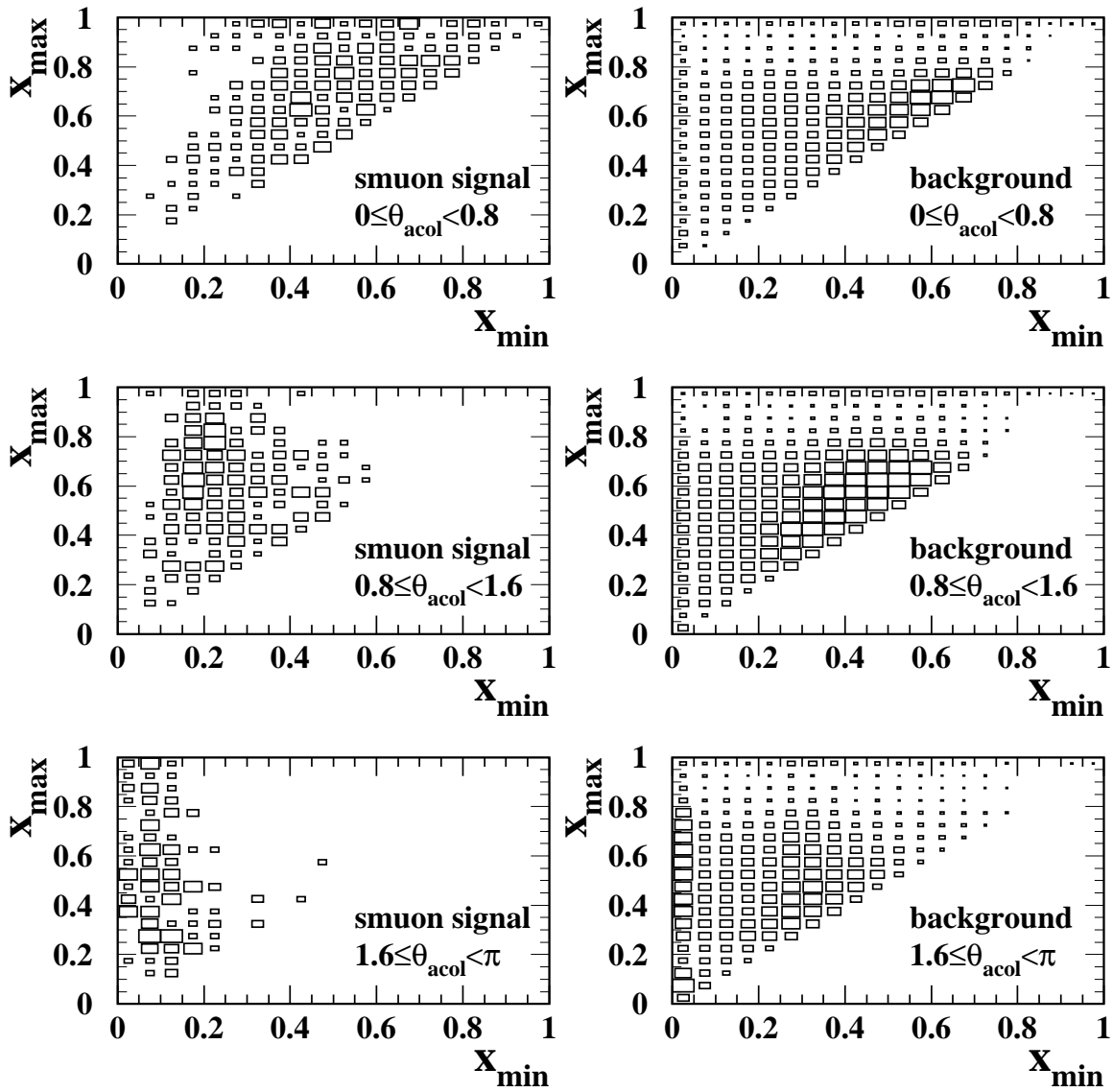


Figure 2: Distributions in the (x_{\min}, x_{\max}) plane, where x_{\min} and x_{\max} are the momenta of the higher and lower momentum lepton respectively, scaled by the beam energy, for three ranges of acolinearity (shown in radians). The distributions are shown for a smuon signal with $m=45$ GeV, $\Delta m=45$ GeV (left), and for Standard Model Monte Carlo (right).

OPAL

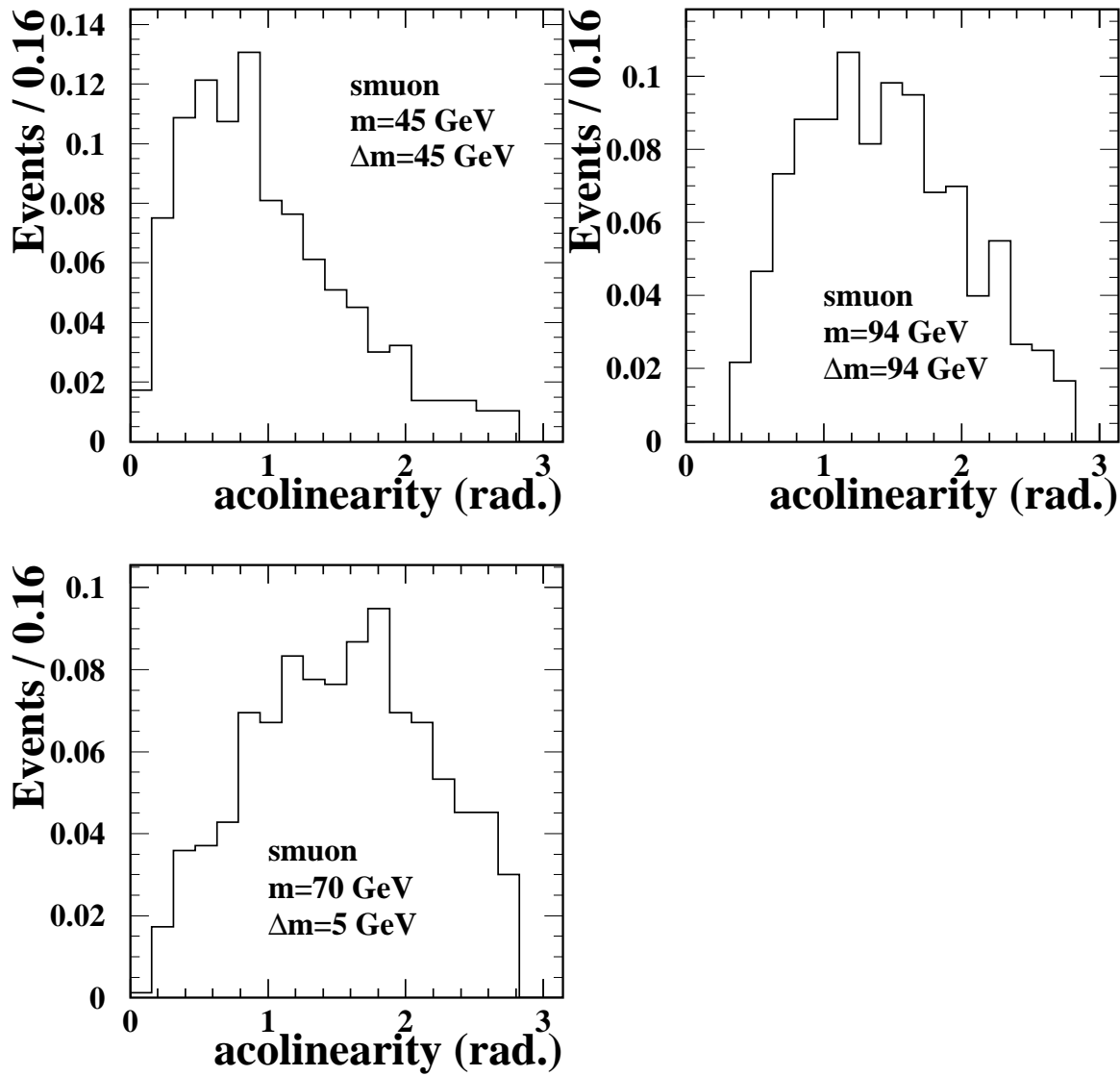


Figure 3: *Distributions of acolinearity (in radians) for three example smuon signals.*

OPAL

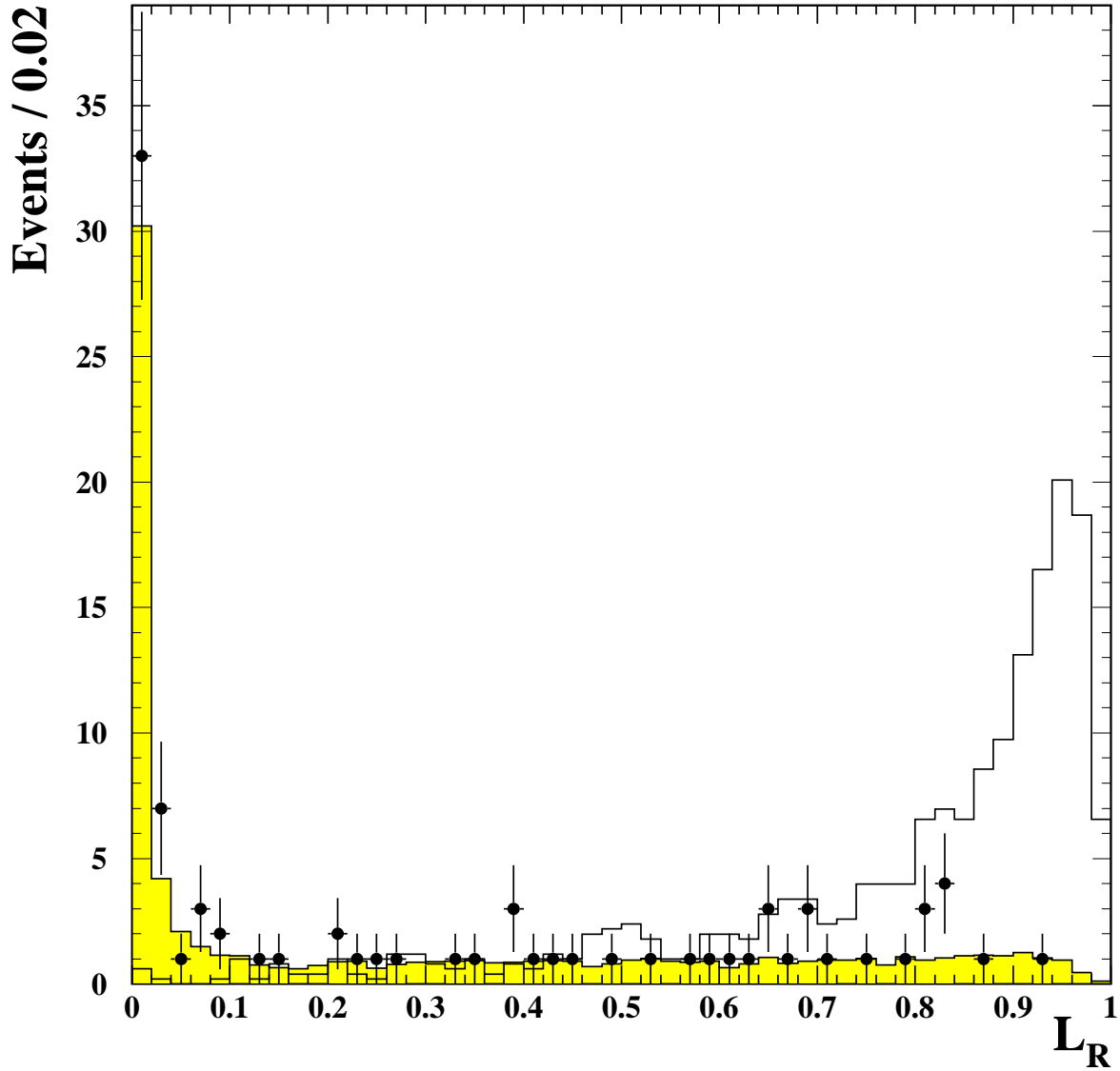


Figure 4: Distributions of the relative likelihood, L_R , for Standard Model Monte Carlo (shaded histogram), signal (open histogram) and data (points with error bars), in the analysis for smuons with a mass of 80 GeV for a smuon-neutralino mass difference of 60 GeV.

OPAL

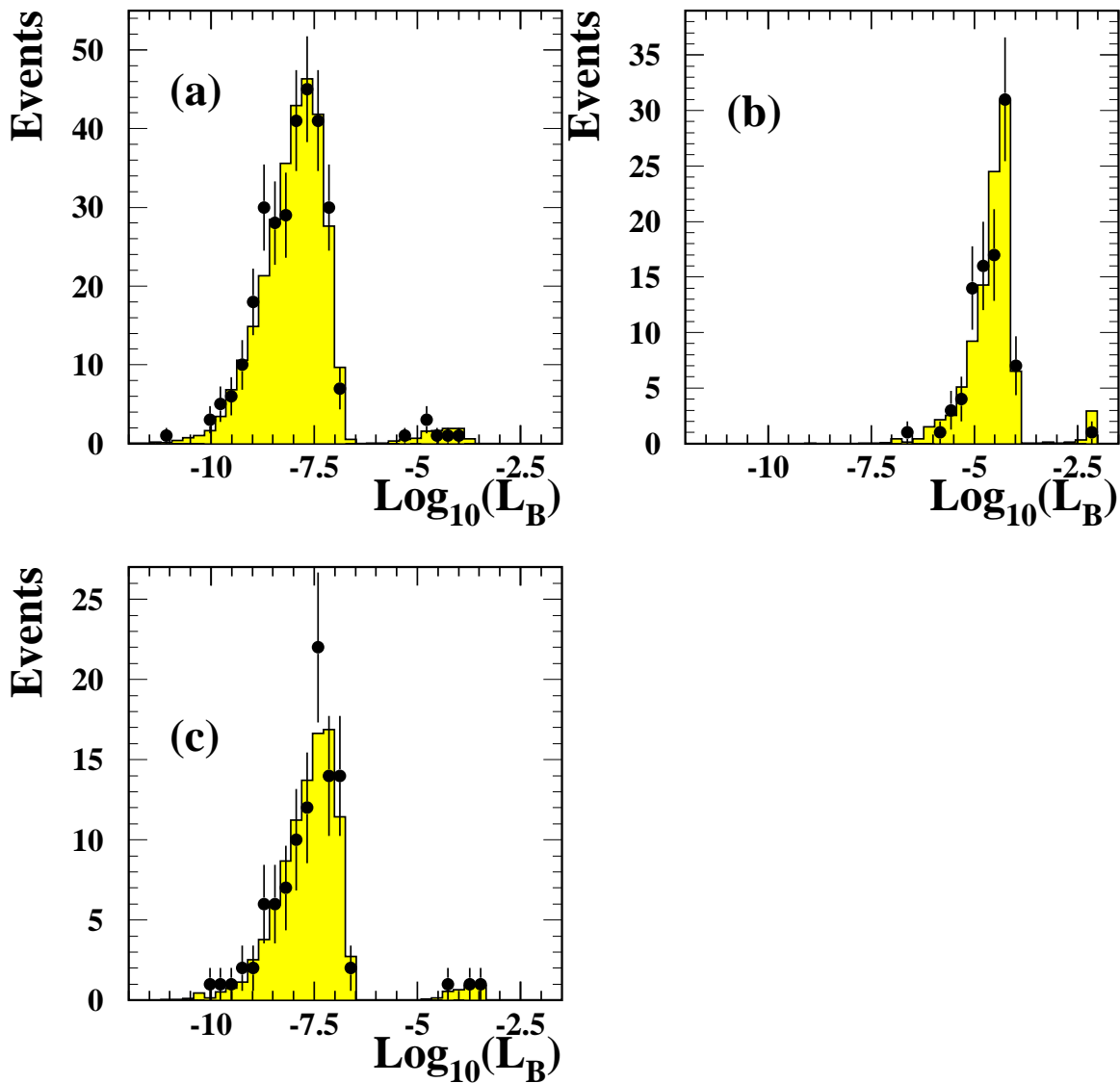


Figure 5: Distributions of the background likelihood, L_B , for Standard Model Monte Carlo (shaded histogram) and data (points with error bars) for events passing the general selection, using all the likelihood variables (a). (b) and (c) show the same information after making the initial lepton identification requirements given in Section 4.4 for the selectron and smuon searches respectively. In (b), only the variables used in the selectron analysis are used.

OPAL

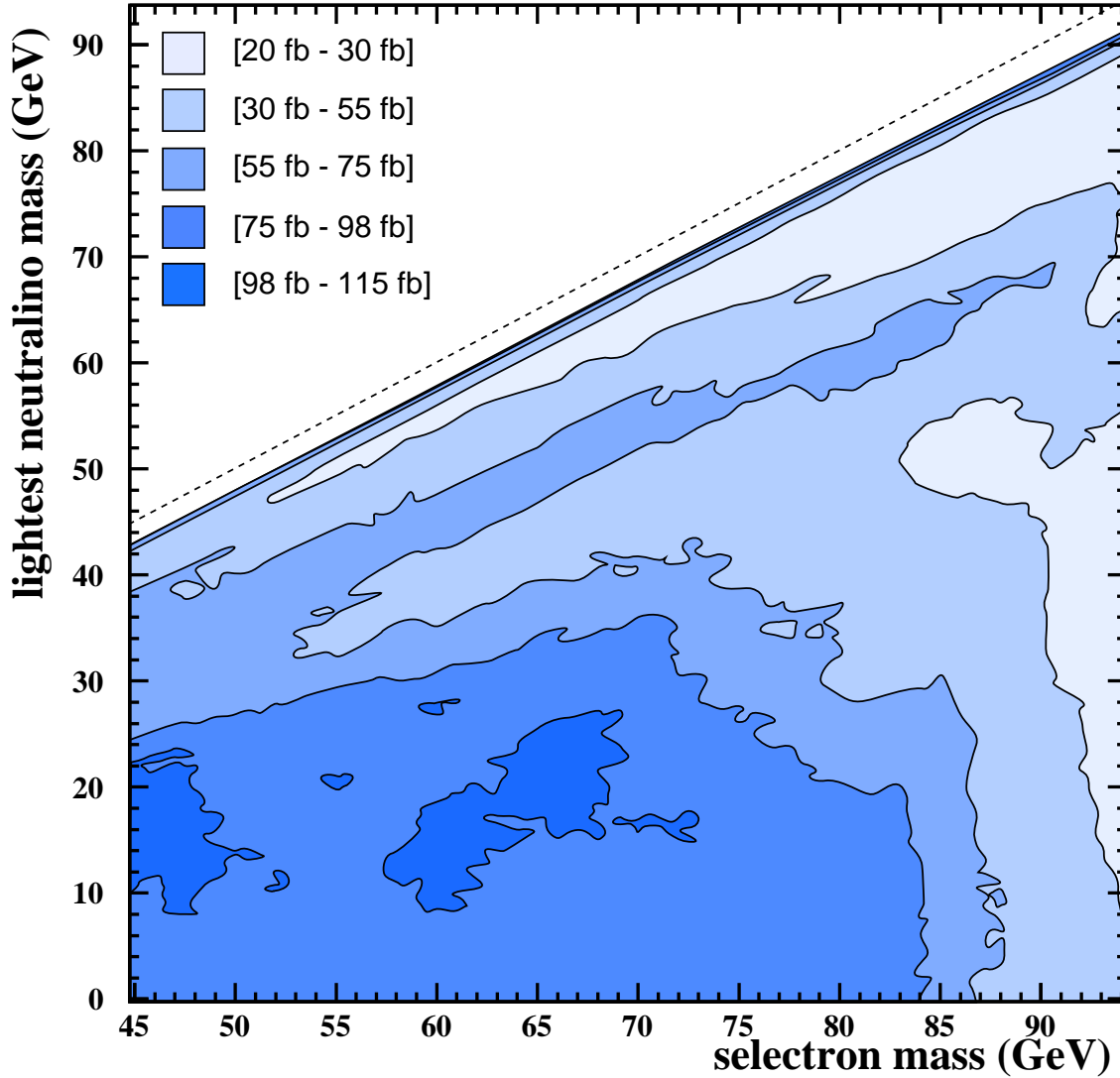


Figure 6: Contours of the 95% CL upper limits on the selectron pair cross-section times $BR^2(\tilde{e} \rightarrow e\tilde{\chi}_1^0)$ at 189 GeV based on combining the 183 and 189 GeV data-sets assuming a β^3/s dependence of the cross-section. The kinematically allowed region is indicated by the dashed line. The unshaded region at very low Δm is experimentally inaccessible in this search.

OPAL

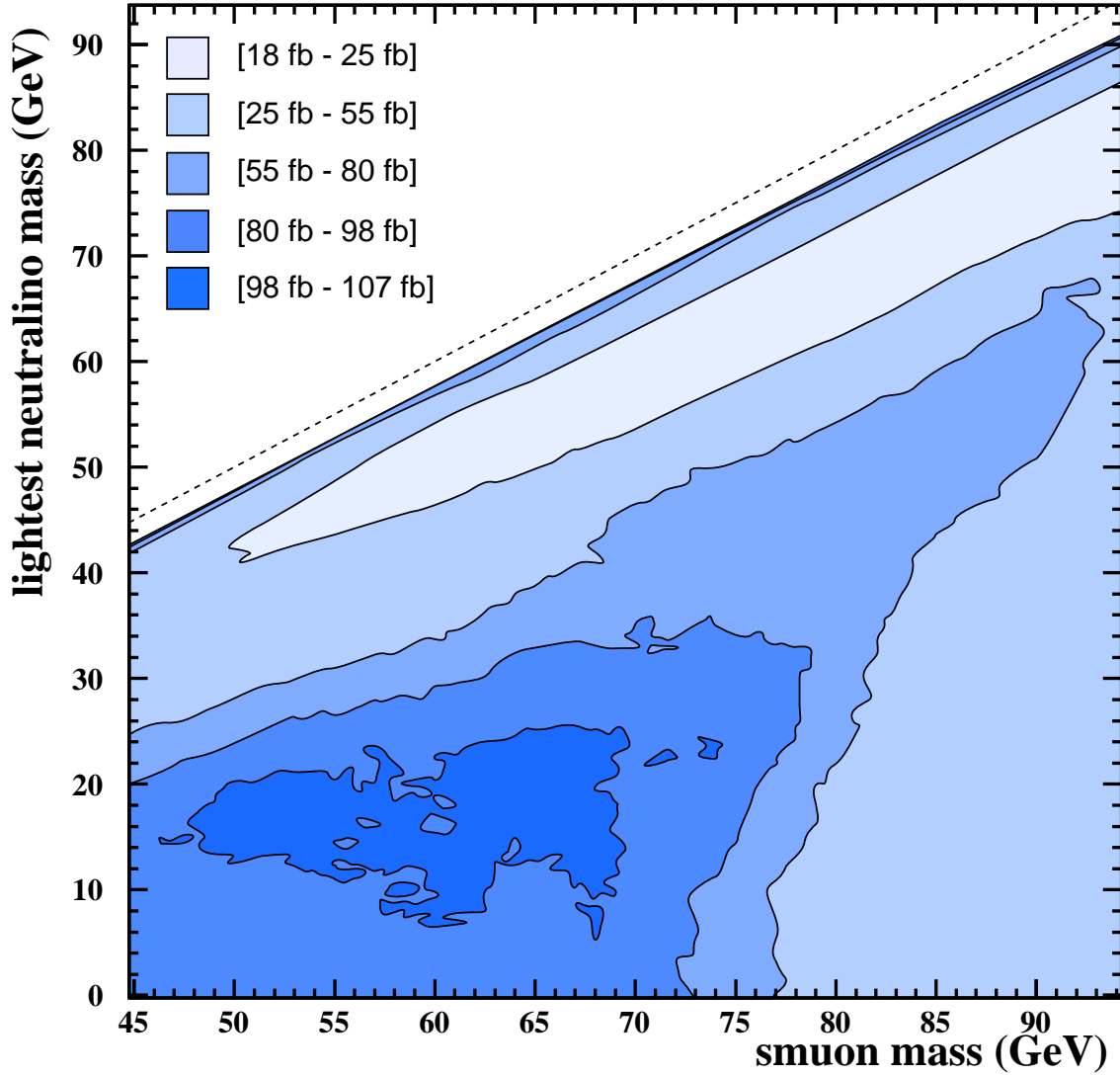


Figure 7: Contours of the 95% CL upper limits on the smuon pair cross-section times $BR^2(\tilde{\mu} \rightarrow \mu\tilde{\chi}_1^0)$ at 189 GeV based on combining the 183 and 189 GeV data-sets assuming a β^3/s dependence of the cross-section. The kinematically allowed region is indicated by the dashed line. The unshaded region at very low Δm is experimentally inaccessible in this search.

OPAL

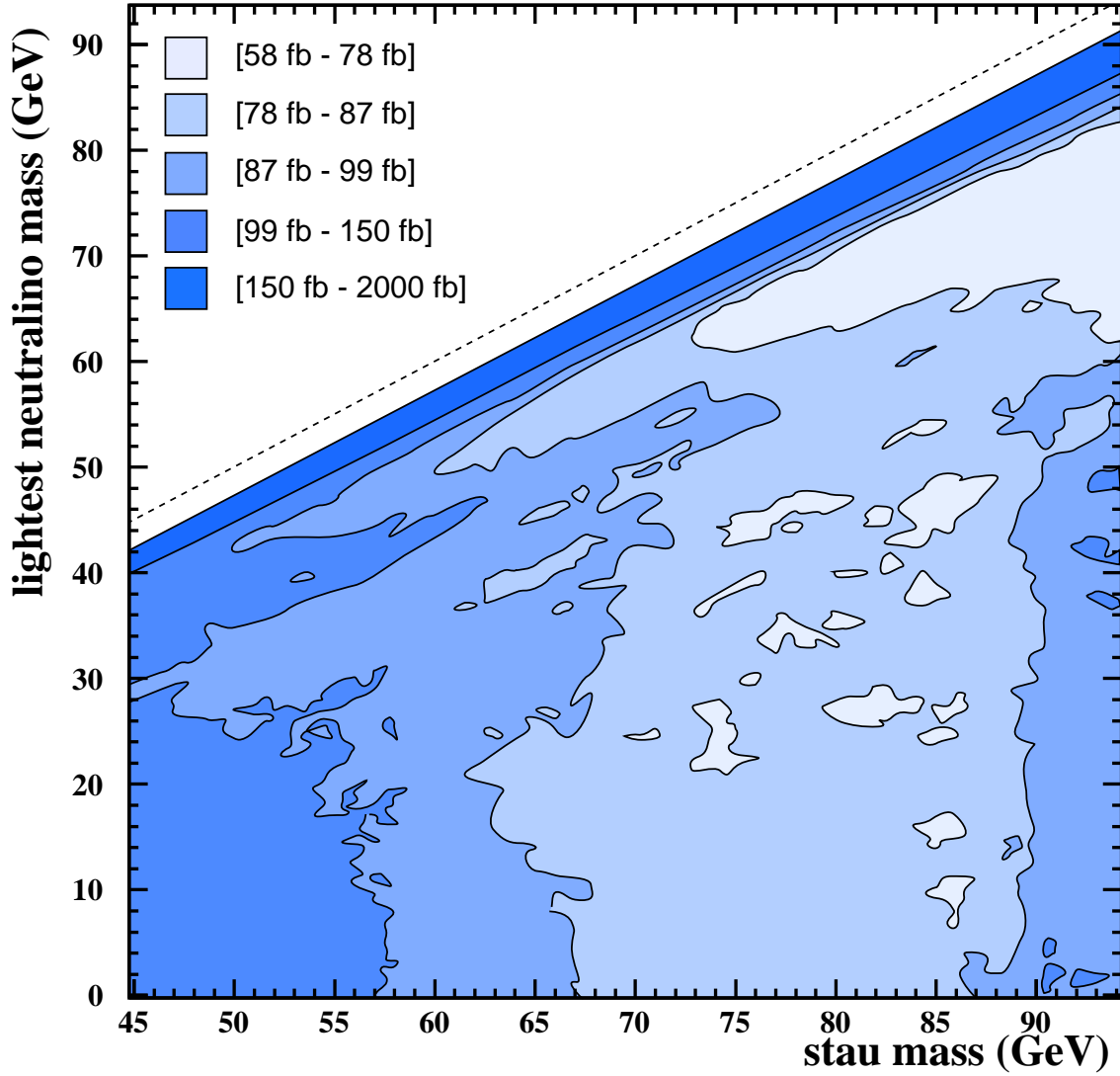


Figure 8: Contours of the 95% CL upper limits on the stau pair cross-section times $BR^2(\tilde{\tau} \rightarrow \tau \tilde{\chi}_1^0)$ at 189 GeV based on combining the 183 and 189 GeV data-sets assuming a β^3/s dependence of the cross-section. The kinematically allowed region is indicated by the dashed line. The unshaded region at very low Δm is experimentally inaccessible in this search.

OPAL

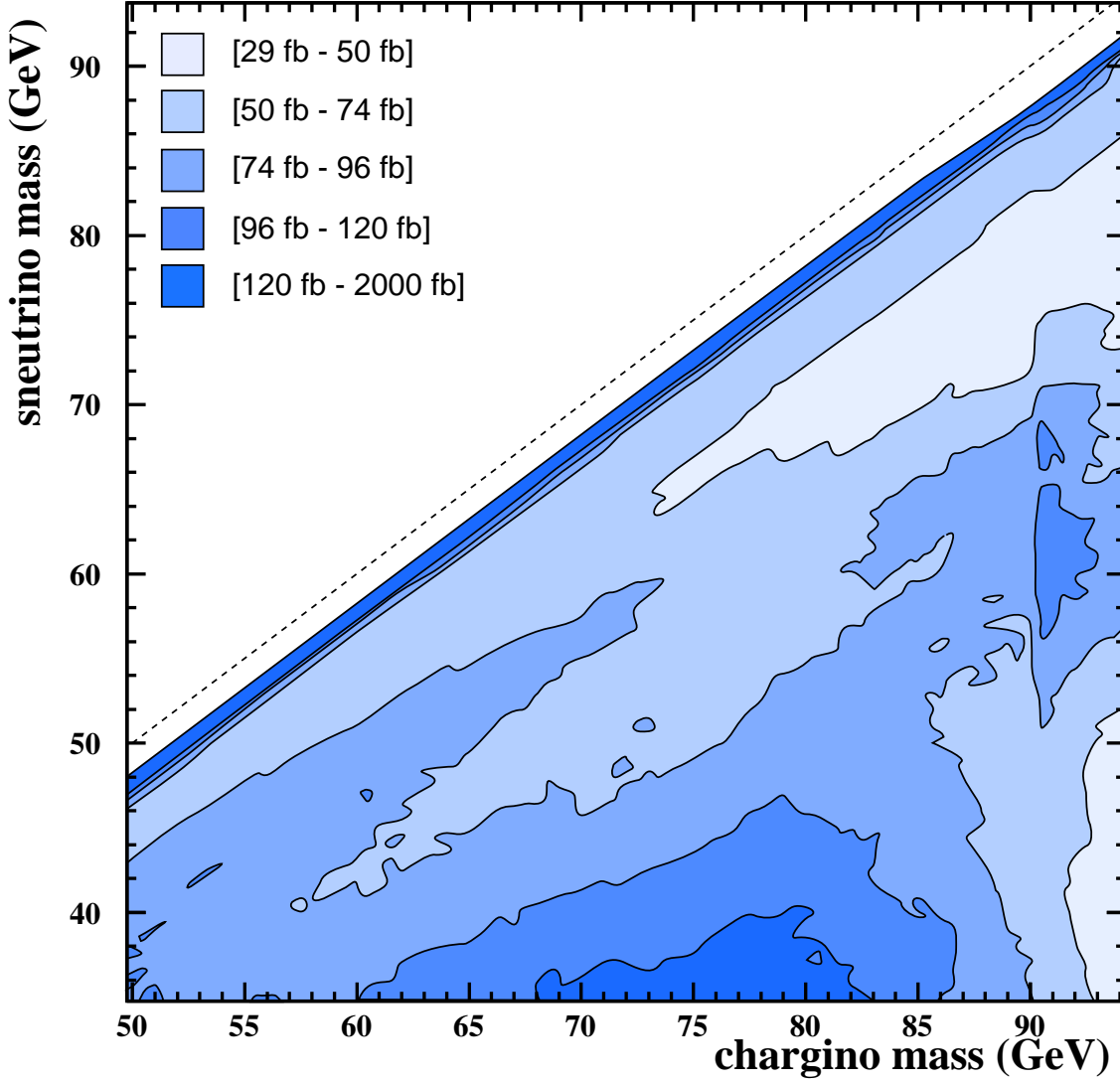


Figure 9: Contours of the 95% CL upper limits on the chargino pair cross-section times branching ratio squared for $\tilde{\chi}_1^\pm \rightarrow \ell^\pm \tilde{\nu}$ (2-body decay) at $\sqrt{s} = 189$ GeV. The limits have been calculated for the case where the three sneutrino generations are mass degenerate. The limit is obtained by combining the 183 and 189 GeV data-sets assuming a β/s dependence of the cross-section. The kinematically allowed region is indicated by the dashed line. The unshaded region at very low Δm is experimentally inaccessible in this search.

OPAL

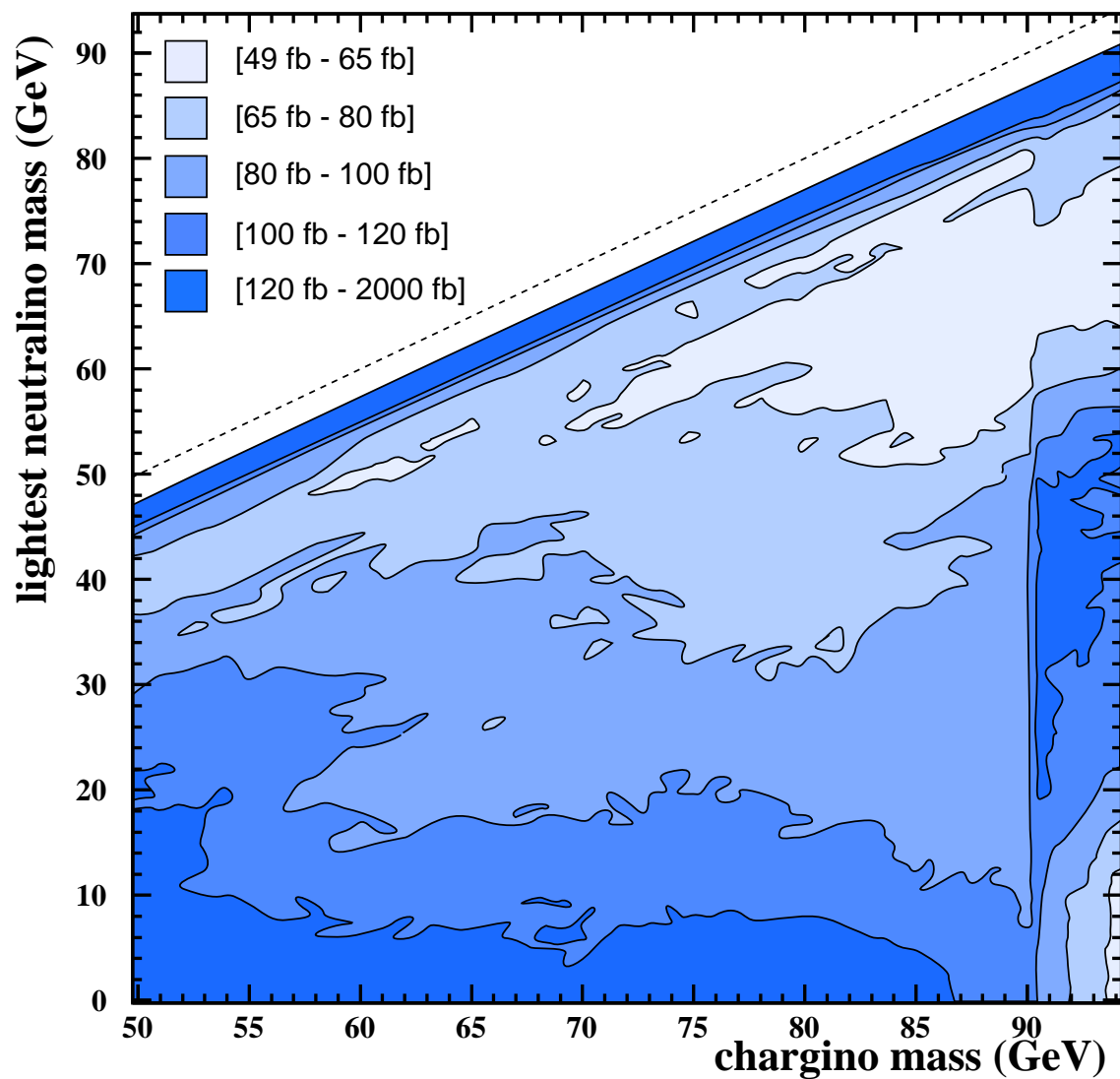


Figure 10: Contours of the 95% CL upper limits on the chargino pair cross-section times branching ratio squared for $\tilde{\chi}_1^\pm \rightarrow \ell^\pm \nu \tilde{\chi}_1^0$ (3-body decay) at $\sqrt{s} = 189$ GeV. The limit is obtained by combining the 183 and 189 GeV data-sets assuming a β/s dependence of the cross-section. The kinematically allowed region is indicated by the dashed line. The unshaded region at very low Δm is experimentally inaccessible in this search.

OPAL

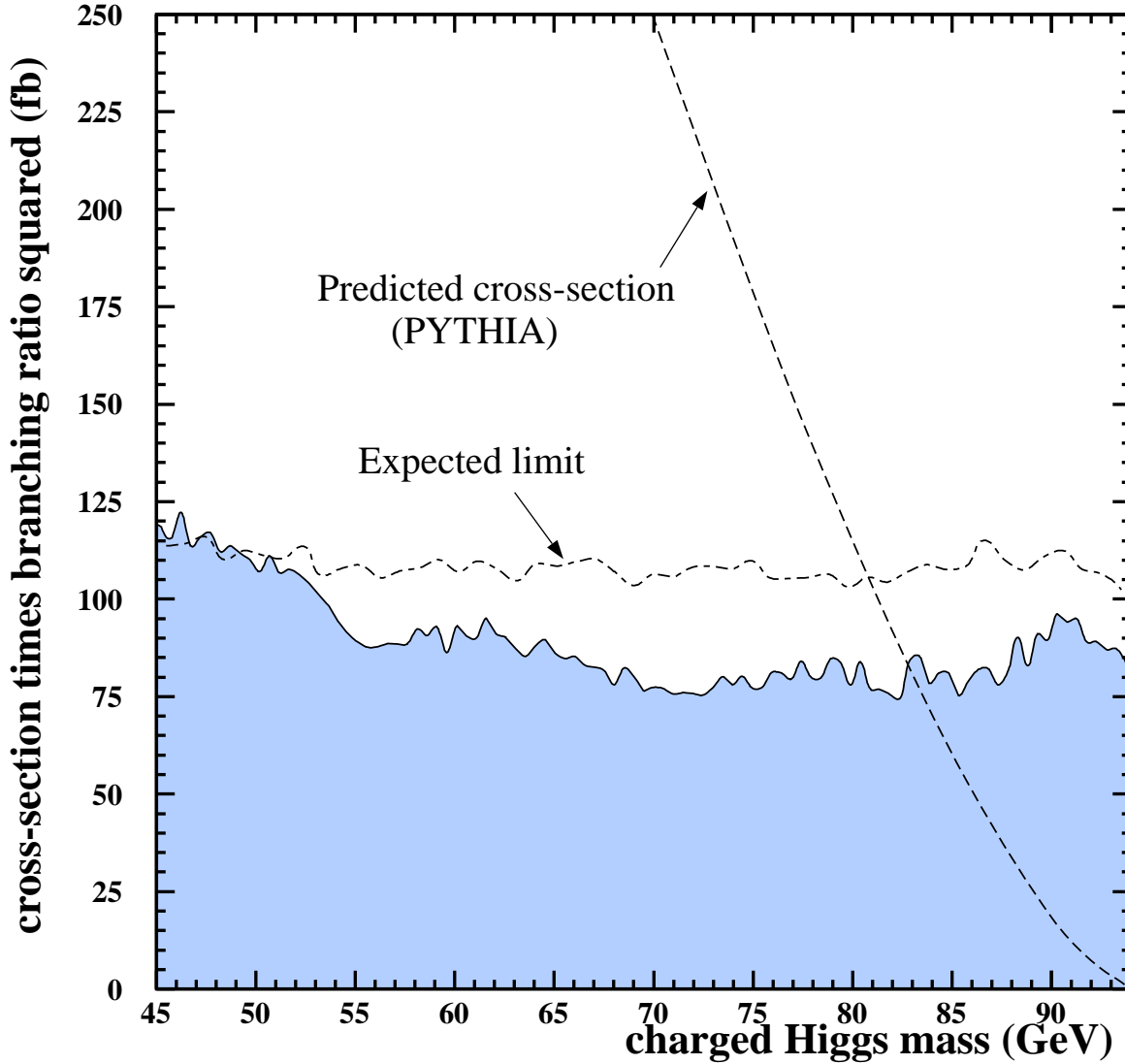


Figure 11: The solid line shows the 95% CL upper limit on the charged Higgs pair production cross-section times branching ratio squared for the decay $H^\pm \rightarrow \tau^\pm \nu_\tau$ at $\sqrt{s} = 189$ GeV. The limit is obtained by combining the 183 and 189 GeV data-sets assuming the m_{H^\pm} and \sqrt{s} dependence of the cross-section predicted by PYTHIA. For comparison, the dashed curve shows the prediction from PYTHIA at $\sqrt{s} = 189$ GeV assuming a 100% branching ratio for the decay $H^\pm \rightarrow \tau^\pm \nu_\tau$. The expected limit calculated from Monte Carlo alone is indicated by the dash-dotted line.

OPAL

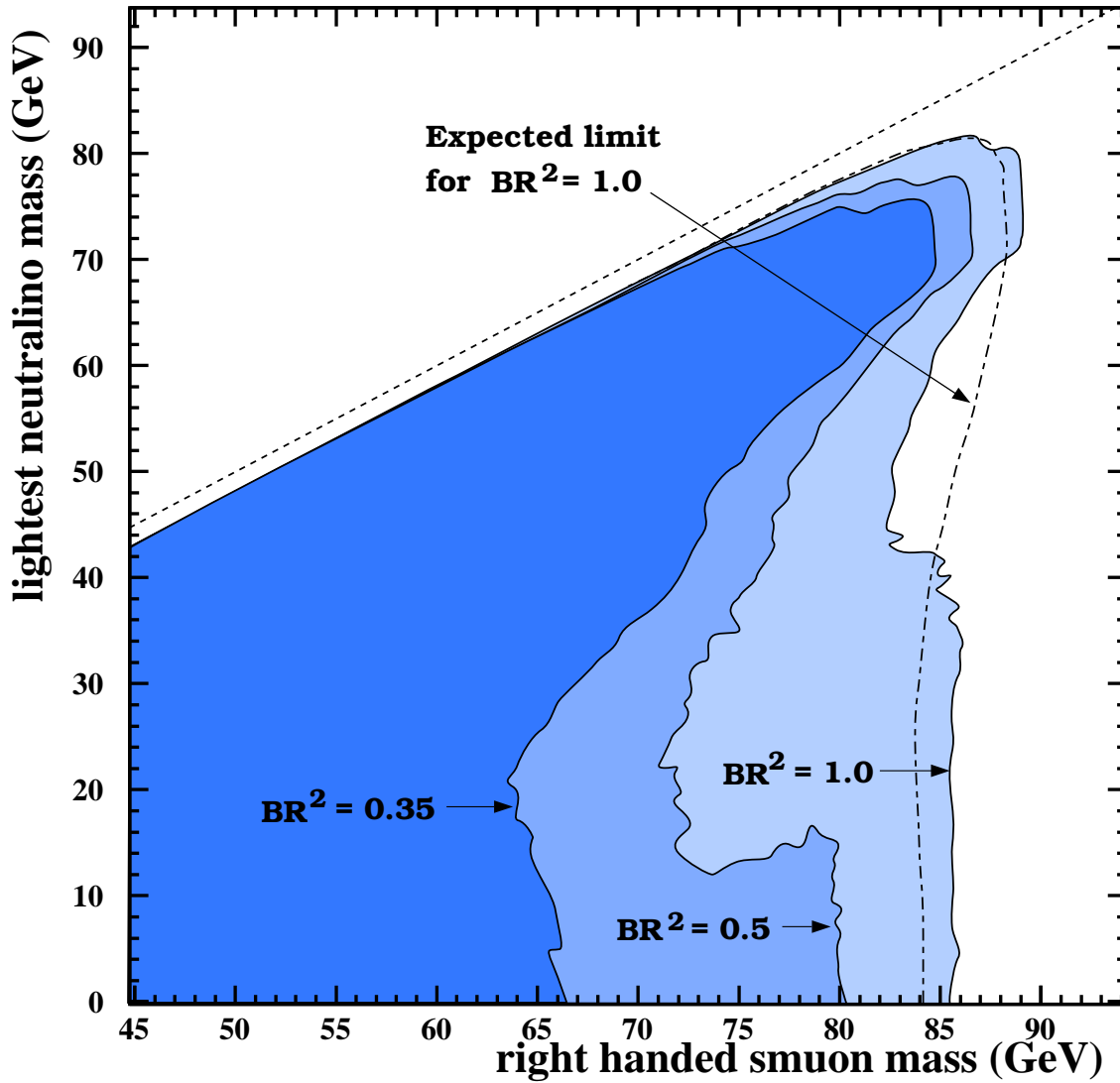


Figure 12: 95% CL exclusion region for right-handed smuon pair production obtained by combining the $\sqrt{s} = 183$ and 189 GeV data-sets. The limits are calculated for several values of the branching ratio squared for $\tilde{\mu}_R^\pm \rightarrow \mu^\pm \tilde{\chi}_1^0$ that are indicated in the figure. Otherwise they have no supersymmetry model assumptions. The kinematically allowed region is indicated by the dashed line. The expected limit for $BR^2 = 1.0$, calculated from Monte Carlo alone, is indicated by the dash-dotted line.

OPAL

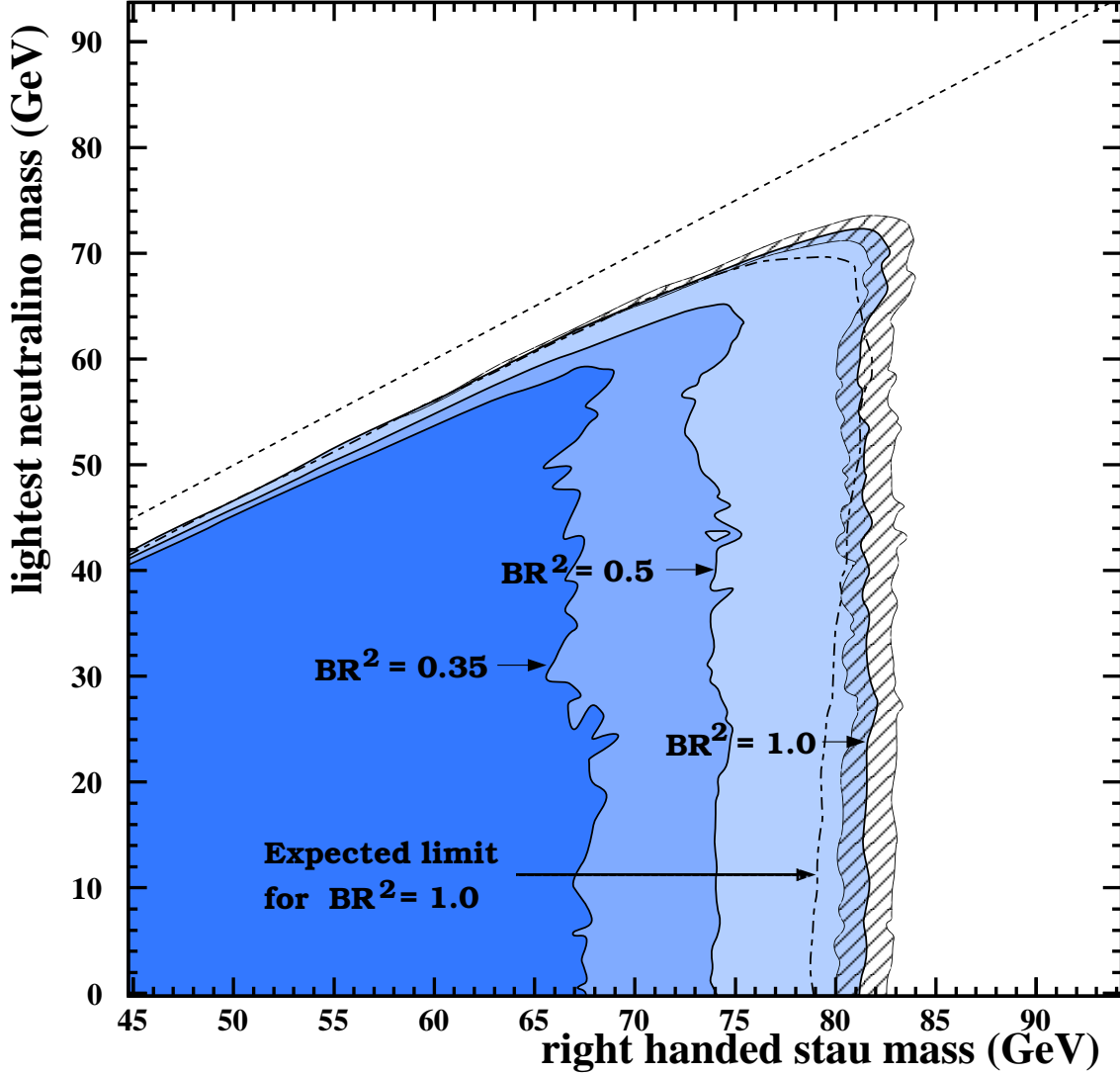


Figure 13: 95% CL exclusion region for right-handed stau pair production obtained by combining the $\sqrt{s} = 183$ and 189 GeV data-sets. The limits are calculated for several values of the branching ratio squared for $\tilde{\tau}_R^\pm \rightarrow \tau^\pm \tilde{\chi}_1^0$. The selection efficiency for $\tilde{\tau}^+ \tilde{\tau}^-$ is calculated for the case that the decay $\tilde{\tau}^- \rightarrow \tau^- \tilde{\chi}_1^0$ produces unpolarised τ^\pm . Otherwise the limits have no supersymmetry model assumptions. The hatched area shows the region in which the limit for $BR^2 = 1.0$ can vary if stau mixing occurs (see text). The kinematically allowed region is indicated by the dashed line. The expected limit for $BR^2 = 1.0$, calculated from Monte Carlo alone, is indicated by the dash-dotted line.

OPAL

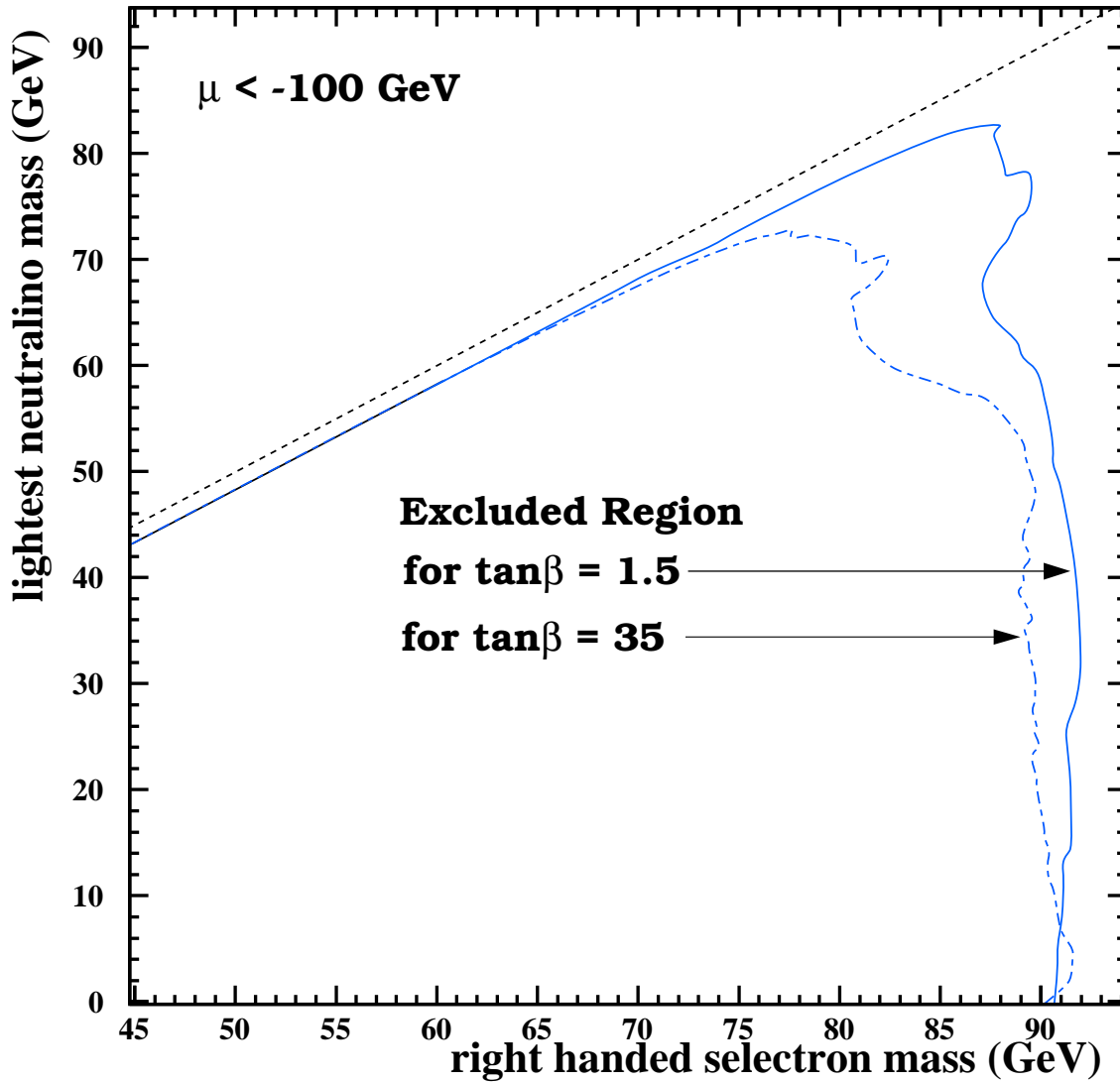


Figure 14: For two values of $\tan\beta$ and $\mu < -100$ GeV, 95% CL exclusion regions for right-handed selectron pairs within the MSSM, obtained by combining the $\sqrt{s} = 183$ and 189 GeV data-sets. The excluded regions are calculated taking into account the predicted branching ratio for $\tilde{e}_R^\pm \rightarrow e^\pm \tilde{\chi}_1^0$. The gauge unification relation, $M_1 = \frac{5}{3} \tan^2 \theta_W M_2$, is assumed in calculating the MSSM cross-sections and branching ratios. The kinematically allowed region is indicated by the dashed line.

OPAL

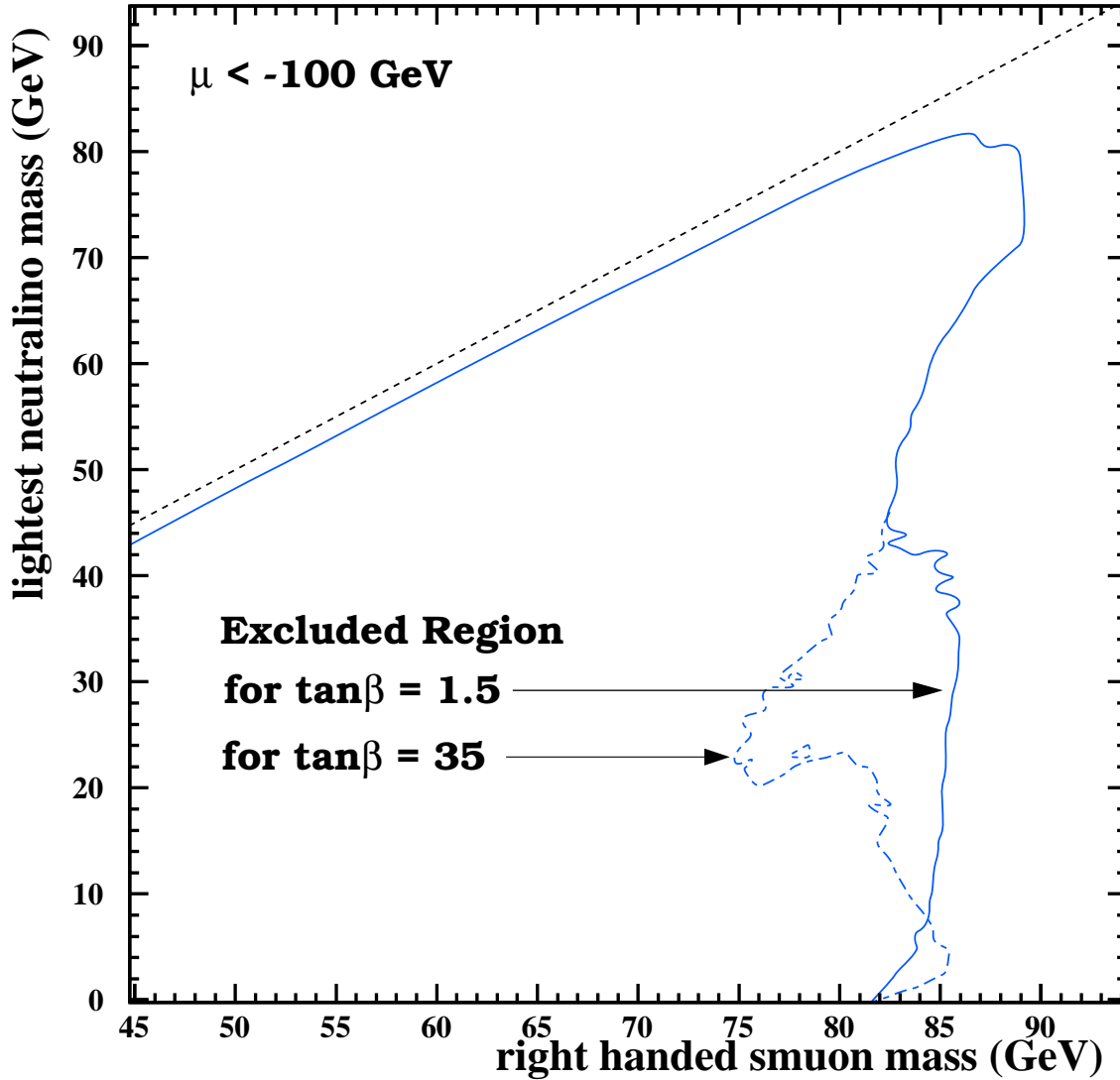


Figure 15: For two values of $\tan\beta$ and $\mu < -100$ GeV, 95% CL exclusion regions for right-handed smuon pairs within the MSSM, obtained by combining the $\sqrt{s} = 183$ and 189 GeV data-sets. The excluded regions are calculated taking into account the predicted branching ratio for $\tilde{\mu}_R^\pm \rightarrow \mu^\pm \tilde{\chi}_1^0$. The gauge unification relation, $M_1 = \frac{5}{3} \tan^2 \theta_W M_2$, is assumed in calculating the MSSM branching ratios. The kinematically allowed region is indicated by the dashed line.

OPAL

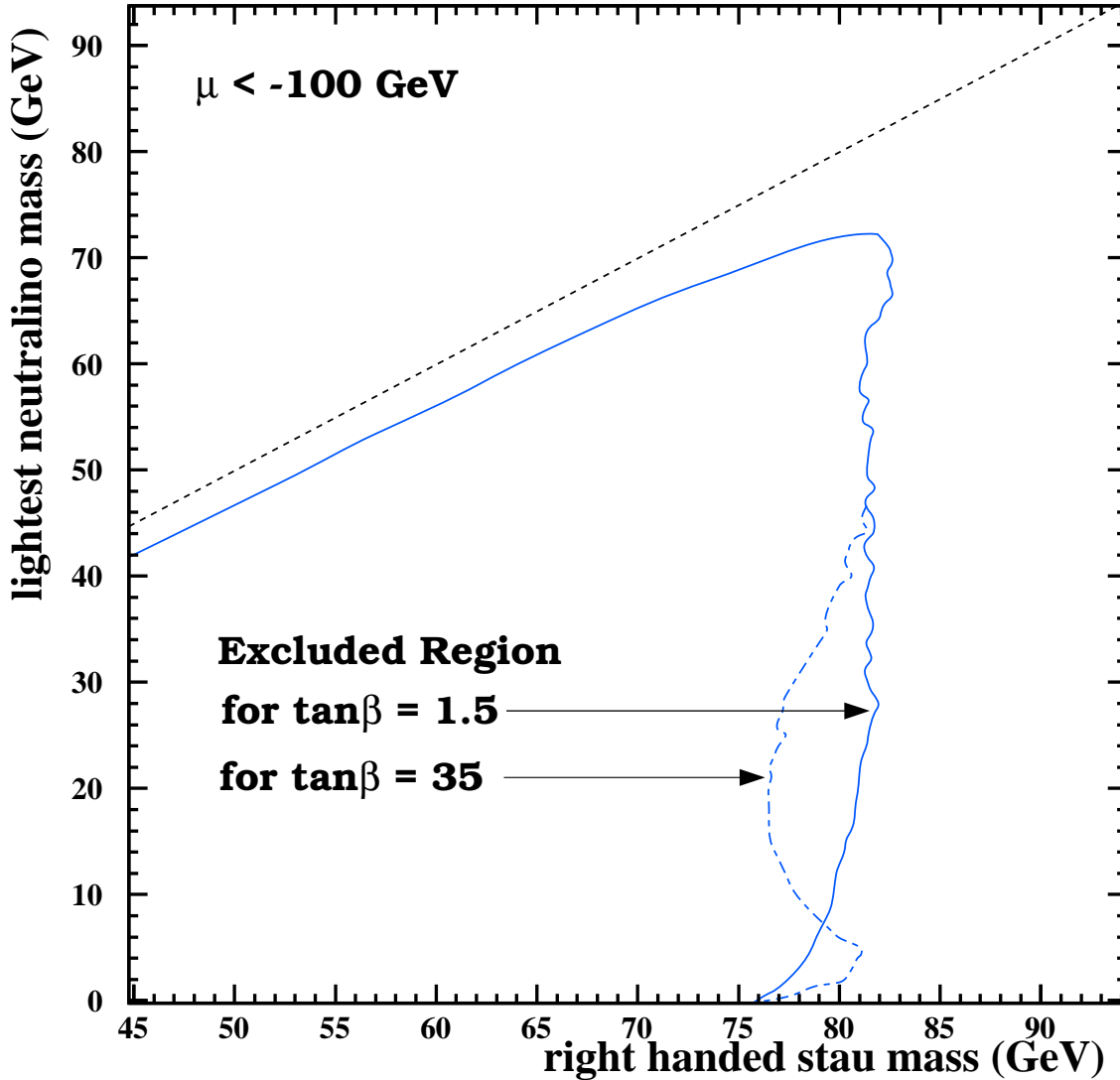


Figure 16: For two values of $\tan\beta$ and $\mu < -100$ GeV, 95% CL exclusion regions for right-handed stau pairs within the MSSM, obtained by combining the $\sqrt{s} = 183$ and 189 GeV data-sets. The excluded regions are calculated taking into account the predicted branching ratio for $\tilde{\tau}_R^\pm \rightarrow \tau^\pm \tilde{\chi}_1^0$. The gauge unification relation, $M_1 = \frac{5}{3} \tan^2 \theta_W M_2$, is assumed in calculating the MSSM branching ratios. The selection efficiency for $\tilde{\tau}^+ \tilde{\tau}^-$ is calculated for the case that the decay $\tilde{\tau}^- \rightarrow \tau^- \tilde{\chi}_1^0$ produces unpolarised τ^\pm . The kinematically allowed region is indicated by the dashed line.